ATLAS CONF Note

ATLAS-CONF-2022-042

11th July 2022

Search for the direct production of charginos and neutralinos in final states with τ-leptons in $\sqrt{s} = 13$ TeV pp collisions with the ATLAS detector

The ATLAS Collaboration

Two searches for the direct production of charginos and neutralinos with intermediate tau sleptons or Wh, in final states with at least two hadronically decaying τ-leptons, are presented. The signal signature also requires an additional isolated light lepton in scenarios in which the charginos and neutralinos decay through an intermediate W or Higgs boson. The analysis uses a dataset of pp collisions corresponding to an integrated luminosity of 139 fb^{-1}, recorded with the ATLAS detector at the Large Hadron Collider at a centre-of-mass energy of 13 TeV. No significant deviation from the expected Standard Model background is observed. Limits are derived in scenarios of $\tilde{\chi}_1^+\tilde{\chi}_1^-$ pair production and of combined $\tilde{\chi}_1^\pm\tilde{\chi}_2^0$ and $\tilde{\chi}_1^+\tilde{\chi}_1^-$ production in simplified models where the neutralinos and charginos decay solely via intermediate left-handed tau sleptons and tau sneutrinos. Chargino masses up to 970 GeV are excluded at 95 % confidence level in the scenario of direct production of $\tilde{\chi}_1^+\tilde{\chi}_1^-$ for a massless $\tilde{\chi}_1^0$. Degenerate $\tilde{\chi}_1^\pm$ and $\tilde{\chi}_2^0$ masses up to 1160 GeV are excluded in the case of production of $\tilde{\chi}_1^\pm\tilde{\chi}_2^0$ and $\tilde{\chi}_1^+\tilde{\chi}_1^-$ via tau sleptons decay assuming a massless $\tilde{\chi}_1^0$. For the $\tilde{\chi}_1^\pm\tilde{\chi}_2^0$ production via an intermediate Wh decay, masses up to 330 GeV are excluded for a massless $\tilde{\chi}_1^0$.

ATLAS-CONF-2022-042
13 July 2022

1 Introduction

Supersymmetry (SUSY) [1–7] postulates the existence of a bosonic (fermionic) partner for each fermionic (bosonic) particle of the Standard Model (SM), whose spin differs by one half unit from each corresponding SM particle. In models that conserve R-parity [8], the lightest supersymmetric particle (LSP) is stable, making it a dark-matter candidate [9, 10].

In the simplified SUSY models considered in this note, the sector of sparticles with only electroweak interactions contains charginos ($\tilde{\chi}_i^{\pm}$, $i = 1, 2$ in order of increasing masses), neutralinos ($\tilde{\chi}_j^0$, $j = 1, 2, 3, 4$ in order of increasing masses), charged sleptons ($\tilde{\ell}$), and sneutrinos ($\tilde{\nu}$). Charginos and neutralinos are the mass eigenstates formed from linear superpositions of the superpartners of the Higgs bosons and electroweak gauge bosons. The charged sleptons are the superpartners of the charged leptons and in a similar convention as for the SM partners, referred to $\tilde{\ell}_{\mathrm{L}}$ or $\tilde{\ell}_{\mathrm{R}}$, respectively. The slepton mass eigenstates are a mixture of $\tilde{\ell}_{\mathrm{L}}$ and $\tilde{\ell}_{\mathrm{R}}$, and are labeled as $\tilde{\ell}_k$ ($k = 1, 2$ in order of increasing mass). In this work, the scalar superpartners of the left-handed τ-lepton (the stau-left, $\tilde{\tau}_{\mathrm{L}}$) and right-handed τ-lepton (the stau-right, $\tilde{\tau}_{\mathrm{R}}$) are assumed to be mass degenerate.

Although they are experimentally challenging, final states with τ-leptons are of particular interest in SUSY searches. Light sleptons could play a role in the co-annihilation of neutralinos in the early universe, and models with light scalar tau slepton decays to light neutralinos can shed light on the nature of dark matter [11]. Furthermore, should SUSY or any other physics beyond the Standard Model (BSM) involving leptons be discovered, independent studies of all three lepton flavours are necessary to investigate the coupling structure of the new physics, especially with regard to lepton universality.

The main signatures studied include those with two hadronically decaying τ-leptons, low jet activity and large missing transverse momentum, $\mathbf{p}_{\mathrm{T}}^{\mathrm{miss}}$, from the neutralinos and neutrinos, referred to as the $\tau_{\mathrm{had}}\tau_{\mathrm{had}}$ channel. In this note, two scenarios are presented. The first scenario includes the production of neutralinos and charginos, $\tilde{\chi}_1^{\pm}\tilde{\chi}_2^0$ (C1N2) and $\tilde{\chi}_1^{+}\tilde{\chi}_1^{-}$ (C1C1), which decay to the lightest neutralino only through intermediate tau sleptons (stau) / tau sneutrinos, denoted as the "Intermediate stau" channel. Additionally, the search for $\tilde{\chi}_1^{\pm}\tilde{\chi}_2^0$ production is separated into final states with two same-sign (SS) or opposite-sign (OS) τ-lepton pairs. The second scenario is the direct production of neutralinos and charginos ($\tilde{\chi}_1^{\pm}\tilde{\chi}_2^0$, C1N2) which decay via the lightest neutral Higgs boson (h), consistent with the SM Higgs boson with a mass of 125 GeV, a W boson and two neutralinos. This scenario is referred to as the "Intermediate Wh" channel. The final state is chosen to contain two hadronic τ-leptons from the Higgs boson decay and one charged light lepton from the W boson decay. Representative Feynman diagrams of the targeted signal processes can be found in Figure 1.

Previous results from ATLAS have set exclusion limits at 95% confidence level on the above SUSY models with the Run-1 and partial Run-2 datasets [12–14]. Chargino masses up to 630 GeV are excluded at 95 % confidence level for $\tilde{\chi}_1^{+}\tilde{\chi}_1^{-}$ production for a massless $\tilde{\chi}_1^0$. Limits on the $\tilde{\chi}_1^{\pm}$ and $\tilde{\chi}_2^0$ masses have been set up to 760 GeV for $\tilde{\chi}_1^{\pm}\tilde{\chi}_2^0$ and $\tilde{\chi}_1^{+}\tilde{\chi}_1^{-}$ for a massless $\tilde{\chi}_1^0$. CMS also set exclusion limits at 95% confidence level on $\tilde{\chi}_1^{\pm}\tilde{\chi}_2^0$ pair production via stau decay using the Run-2 dataset [15]. In the CMS result, chargino and neutralino masses up to 980 GeV are excluded for a massless lightest neutralino. This search aims to extend the current ATLAS reach to higher chargino masses and smaller mass differences between $\tilde{\chi}_2^0$ / $\tilde{\chi}_1^{\pm}$ and $\tilde{\chi}_1^0$ using the full Run-2 dataset.

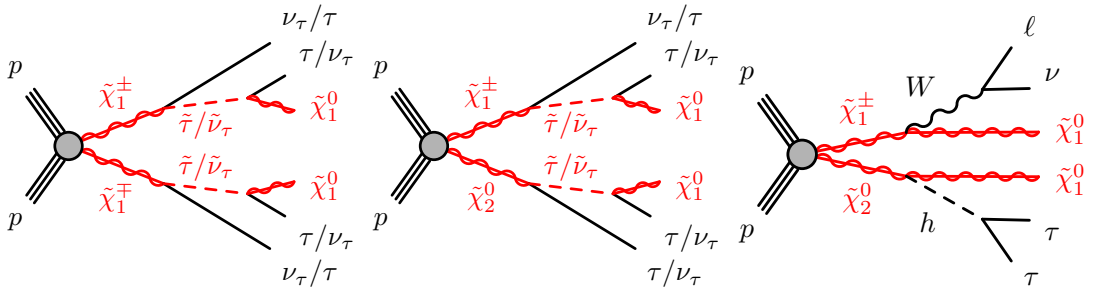

Figure 1: Representative Feynman diagrams of SUSY scenarios which are being searched for in this note. In all cases, the subsequent decays contain a two τ-lepton final state. In the case of $\tilde{\chi}_1^{\pm}\tilde{\chi}_2^0$ production (b), the final state can contain more than two τ-leptons.

2 ATLAS detector

The ATLAS experiment [16] at the LHC is a multipurpose particle detector with a forward–backward symmetric cylindrical geometry and a near 4π coverage in solid angle.[1] It consists of an inner tracking detector (ID) surrounded by a thin superconducting solenoid providing a 2 T axial magnetic field, electromagnetic and hadron calorimeters, and a muon spectrometer. The inner tracking detector covers the pseudorapidity range $|\eta| < 2.5$. It consists of silicon pixel, silicon microstrip, and transition radiation tracking detectors. Lead/liquid-argon (LAr) sampling calorimeters provide electromagnetic (EM) energy measurements with high granularity. A steel/scintillator-tile hadron calorimeter covers the central pseudorapidity range ($|\eta| < 1.7$). The endcap and forward regions are instrumented with LAr calorimeters for both the EM and hadronic energy measurements up to $|\eta| = 4.9$. The muon spectrometer (MS) surrounds the calorimeters and is based on three large superconducting air-core toroidal magnets with eight coils each. The field integral of the toroids ranges between 2.0 and 6.0 T m across most of the detector. The muon spectrometer includes a system of precision tracking chambers and fast detectors for triggering. A two-level trigger system is used to select events. The first-level trigger is implemented in hardware and uses a subset of the detector information to accept events at a rate below 100 kHz. This is followed by a software-based trigger that reduces the accepted event rate to 1 kHz on average depending on the data-taking conditions. An extensive software suite [17] is used in the reconstruction and analysis of real and simulated data, in detector operations, and in the trigger and data acquisition systems of the experiment.

[1] ATLAS uses a right-handed coordinate system with its origin at the nominal interaction point (IP) in the centre of the detector and the z-axis along the beam pipe. The x-axis points from the IP to the centre of the LHC ring, and the y-axis points upwards. Cylindrical coordinates (r, ϕ) are used in the transverse plane, ϕ being the azimuthal angle around the z-axis. The pseudorapidity is defined in terms of the polar angle θ as $\eta = -\ln\tan(\theta/2)$. Angular distance is measured in units of $\Delta R \equiv \sqrt{(\Delta\eta)^2 + (\Delta\phi)^2}$.

3 Data and simulated event samples

3.1 Data

The dataset considered in this note corresponds to 139 fb^{-1} of pp LHC collision data collected between 2015 and 2018 by the ATLAS detector, at a centre-of-mass energy of 13 TeV and with a 25 ns proton bunch crossing interval. The uncertainty on the combined 2015–2018 integrated luminosity was measured to be 1.7% [18], obtained using the LUCID-2 detector [19] for the primary luminosity measurements. Data quality requirements are imposed to ensure that only events in which the entire ATLAS detector was functioning well are used [20].

3.2 Monte Carlo simulations

Simulated events produced with several Monte Carlo (MC) event generators are used to predict yields for background contributions from Standard Model (SM) processes and for possible SUSY signals.

All simulated events are overlaid with multiple pp collisions simulated with the soft QCD processes of Pythia 8.186 [21] using the A3 set of tuned parameters [22] and the NNPDF2.3 leading order (LO) parton distribution functions (PDFs) [23]. The simulated events are weighted such that the pile-up conditions match those of the data and are required to pass the trigger selections. The response of the detector to particles was modelled with an ATLAS detector simulation [24] based on Geant4 [25], or using fast simulation based on a parameterisation of the performance of the ATLAS EM and hadronic calorimeters [26] and on Geant4 elsewhere.

3.2.1 Simulated background samples

Final states with two hadronically decaying τ-leptons, low jet activity and a large $\mathbf{p}_{\mathrm{T}}^{\mathrm{miss}}$ are included in this analysis. As a result, SM backgrounds containing both real and misidentified τ-lepton contributions are included. These backgrounds are summarised in the following.

The production of top-quark pairs ($t\bar{t}$) and single top quarks in the Wt and s-channels was performed with Powheg-Box v2 [27–30], with the NNPDF2.3LO [23] PDF set at NLO in the Matrix elements (ME) calculations and the ATLAS underlying-event tune A14 [31]. Electroweak t-channel single-top-quark events were generated using the Powheg-Box v2 event generator. The parton shower (PS), fragmentation, and the underlying event were simulated using Pythia 8.186 with the NNPDF2.3LO PDF set and a corresponding set of A14 tuned parameters. The top-quark mass was set to 172.5 GeV. The $t\bar{t}$ sample was normalised to the cross-section prediction at next-to-next-to-leading order (NNLO) in QCD including the resummation of next-to-next-to-leading logarithmic (NNLL) soft-gluon terms calculated using Top++2.0 [32–38]. The cross-section for single-top-quark was computed for the Wt-channel at NLO in QCD with NNLL soft gluon corrections [39, 40], and to NLO in QCD for the t- and s-channels [39, 40]. Top-quark pair production with an additional W or Z boson was calculated using MadGraph5_aMC@NLO 2.2.2 [41] at NLO in the ME calculations, while fragmentation and hadronisation were simulated with Pythia 8.186. The underlying-event tune A14 was used with the NNPDF2.3LO PDF set, and the cross-sections were normalised using NLO predictions [42, 43].

Events with $Z/\gamma^* \to \ell\ell$ ($\ell = e, \mu, \tau$) and $W \to \ell\nu$ produced in association jets (including jets initiated by heavy flavour quarks) were generated with Sherpa 2.2.1 [44, 45]. ME were calculated for up to two additional partons at NLO and four additional partons at LO, using the Comix [46] and OpenLoops [47, 48] generators and merged with the Sherpa PS [49] using the ME+PS@NLO prescription [45]. The NNPDF3.0NNLO [50] PDF set was used in conjunction with a dedicated PS tuning developed by the Sherpa authors. The W/Z+jets events were normalized using their next-to-next-to-leading-order (NNLO) cross-sections [51].

Fully leptonically and semileptonically decaying diboson samples ($VV = WW/WZ/ZZ$) were simulated with the Sherpa 2.2.1 and 2.2.2 [44] generator at NLO. In this setup, multiple matrix elements were matched and merged with the Sherpa parton shower based on Catani–Seymour dipole factorization [49] using the MEPS@NLO prescription [45, 52–54]. The virtual QCD corrections for matrix elements at NLO accuracy were provided by the OpenLoops library [48]. Samples were generated using the NNPDF3.0NNLO set, along with the dedicated set of tuned parton-shower parameters developed by the Sherpa authors.

Contributions from Higgs boson events produced by gluon–gluon fusion and vector-boson fusion were modelled using Powheg-Box v2 with the NNPDF3.0NNLO PDF and showered using Pythia 8.186. Associated production of a Higgs boson with a vector boson and a Higgs boson in association with two top quarks were simulated using Pythia 8.186 and MadGraph5_aMC@NLO, respectively. All Higgs boson samples were normalised to the cross-sections from Ref. [55].

For all samples showered with Pythia 8, EvtGen 1.2.0 [56] was used to simulate the decays of bottom and charmed hadrons.

3.2.2 Simulated signal samples

SUSY signal model samples were generated to allow the interpretation of the search results in terms of SUSY parameters and were simulated using the ATLAS fast detector simulation. Signal samples were generated using MadGraph5_aMC@NLO 2.2.3 interfaced to Pythia 8.186 with the A14 tune for the PS modelling, hadronisation, and underlying event. The ME calculation was performed at tree level and includes the emission of up to two additional partons. The PDF set used for the generation was NNPDF2.3LO. The ME–PS merging used the CKKW-L [57] prescription, with a matching scale set to one quarter of the mass of the pair of produced particles. Signal cross-sections were calculated with Resummino v2.0.1 to next-to-leading order in the strong coupling constant, adding the resummation of soft gluon emission at next-to-leading-logarithm accuracy (NLO+NLL) [58, 59]. The nominal cross-section and the uncertainty were taken from an envelope of cross-section predictions using different PDF sets and factorisation and renormalisation scales, as described in Ref. [60].

4 Event reconstruction

After the data quality requirements mentioned in Section 3.1 have been applied, events with at least one reconstructed primary vertex [61] are selected. A primary vertex is defined to have at least two associated charged-particle tracks with transverse momentum $p_{\mathrm{T}} > 400$ MeV and be consistent with the beam spot envelope. If there are multiple primary vertices in an event, the one with the largest $\sum p_{\mathrm{T}}^2$ of the associated tracks is chosen.

Jets are reconstructed from particle-flow objects calibrated at the electromagnetic scale [62] using the anti-k_t algorithm [63, 64] with a radius parameter of 0.4. Jet energies are corrected for detector inhomogeneities, the non-compensating response of the calorimeter, and the impact of pile-up [65, 66]. The impact due to pile-up is accounted for using a technique based on jet areas, that provides an event-by-event and jet-by-jet correction [67]. Such jets that are likely to have originated from pile-up are not considered [68]. Jets are required to have $p_{\mathrm{T}} > 20$ GeV and $|\eta| < 2.8$ and events containing jets that are likely to have arisen from detector noise or cosmic rays are removed.

Jets containing b-hadrons (b-jets) are identified using the "DL1" algorithm [69], a multivariate discriminant making use of track impact parameters and reconstructed secondary vertices. Candidate b-jets are required to have $|\eta| < 2.5$. A working point with an average b-tagging efficiency of 77 % for simulated $t\bar{t}$ events is used.

Electron candidates are reconstructed by matching clusters in the electromagnetic calorimeter with charged-particle tracks in the inner detector. Electrons are required to have $p_{\mathrm{T}} >10$ GeV, $|\eta| < 2.47$, and to satisfy the "loose" working point according to a likelihood-based identification algorithm [70]. Muon candidates are reconstructed from MS tracks matching ID tracks. Muons are required to have $p_{\mathrm{T}} > 10$ GeV and $|\eta| < 2.7$ and fulfil the "medium" quality criteria of Ref. [71]. Events containing a muon candidate with a poorly measured charge-to-momentum ratio ($\sigma(q/p) \,/\, |q/p| > 0.2$) are rejected. Events are required not to contain any candidate muon with large transverse (d_0) and longitudinal (z_0) impact parameter, $|z_0| > 1$ mm or $|d_0| > 0.2$ mm, in order to reduce contributions from those originating from cosmic rays. The efficiencies for electrons and muons to satisfy the reconstruction, identification, and isolation criteria are measured in samples of leptonic Z and J/ψ decays, and corrections are applied to the simulated samples to reproduce the efficiencies observed in data.

The reconstruction of hadronically decaying τ-leptons is based on information from tracks in the ID and three-dimensional clusters in the electromagnetic and hadronic calorimeters. The tau reconstruction algorithm is seeded by jets reconstructed from topological clusters of energy deposits in the calorimeter and use a looser requirement of $p_{\mathrm{T}} >10$ GeV and $|\eta| < 2.5$. The reconstructed energies of the hadronically decaying τ-lepton candidates are corrected to the tau energy scale, which is calibrated based on simulation and in-situ measurements using $Z \rightarrow \tau\tau$ decays [72]. Hadronic tau-decay candidates are required to have one or three associated charged-particle tracks (prongs) and the total electric charge of those tracks must be ± 1 times the electron charge. To improve the discrimination between hadronically decaying τ-leptons and jets, electrons, or muons, multivariate algorithms are used [73]. A recursive neural network discriminant is used to reject jets that do not originate from a hadronically decaying τ-lepton with a "medium" or "tight" working point [74]. A boosted decision tree is used to discriminate 1-prong τ-lepton candidates against electrons. This discriminant is built using information from the calorimeter and the tracking detector. This requirement has about 95 % efficiency, and a rejection factor from 10 to 50 depending on the η range. τ-lepton candidates are required to have $p_{\mathrm{T}} > 20$ GeV and $|\eta| < 2.47$, and must lie outside the transition region between the barrel and end-cap calorimeters ($1.37 < |\eta| < 1.52$).

The simulation is corrected for differences in the efficiencies of the tau identification at both trigger and reconstruction level between data and simulation. For hadronically decaying τ-leptons originating from prompt gauge boson decays, the corrections are calculated with a *tag-and-probe* method in a sample of $Z \rightarrow \tau\tau$ events where one τ-lepton decays hadronically and the other leptonically into a muon and two neutrinos [75].

The measured $\mathbf{p}_{\mathrm{T}}^{\mathrm{miss}}$, and its magnitude $E_{\mathrm{T}}^{\mathrm{miss}}$, is based on the negative vectorial sum of the $\mathbf{p}_{\mathrm{T}}$ of all identified jets, τ-lepton candidates, electrons, photons, muons, and an additional soft term. The soft term

is constructed from all tracks that are associated with the primary vertex but not with any identified particle or jet [76, 77].

The possible double counting of reconstructed objects is resolved in the following order. The τ-lepton candidates that are close to electron or muon candidates ($\Delta R < 0.2$, where $\Delta R = \sqrt{(\Delta y)^2 + (\Delta\phi)^2}$) are removed, as are electrons that share a track with a muon. For electrons close to a jet ($\Delta R < 0.4$), the electron is removed, except when $\Delta R < 0.2$ and the jet is not b-tagged, in which case the jet is removed. Any remaining jet within $\Delta R = 0.4$ of a muon or τ-lepton candidate is removed.

5 General analysis strategy and event variables

Events for all scenarios are required to have at least two hadronically decaying τ-leptons. Signal regions (SR) are defined to target the specific SUSY scenario, using kinematic variables with good signal−to−background separation, described in this section. For τ-leptons, kinematic variables are calculated from the visible decay products. The event selections and background estimations are described for the intermediate stau channel in Section 6 and the intermediate Wh channel in Section 7.

The main SM backgrounds are estimated by normalising MC simulation samples to data in dedicated control regions (CRs); backgrounds resulting from non-prompt and misidentified leptons are derived from data, while sub-dominant backgrounds are estimated using MC simulation only. To validate the modelling of the SM backgrounds, the yields and shapes of key kinematic variables are compared to data in dedicated validation regions (VR).

The following variables are used to discriminate SUSY signals from the SM background:

- the "stransverse mass", m_{T2}, which has a kinematic endpoint for events where two massive pair produced particles each decay to two objects, one of which is detected (the lepton in our case) and the other escapes undetected (the neutralino) [78, 79]. It is defined as:

$$m_{\mathrm{T2}} = \min_{\mathbf{q}_{\mathrm{T}}} \left[\max \left(m_{\mathrm{T1}}(\mathbf{p}_{\mathrm{T1}}, \mathbf{q}_{\mathrm{T}}), m_{\mathrm{T2}}(\mathbf{p}_{\mathrm{T2}}, \mathbf{p}_{\mathrm{T}}^{\mathrm{miss}} - \mathbf{q}_{\mathrm{T}}) \right) \right],$$

  where $\mathbf{p}_{\mathrm{T1}}$ and $\mathbf{p}_{\mathrm{T2}}$ are the transverse momenta of the two leptons and and $\mathbf{q}_{\mathrm{T}}$ is the transverse vector chosen to minimize the larger of the two transverse masses, m_{T1} and m_{T2}. They are defined by

$$m_{\mathrm{T}}(\mathbf{p}_{\mathrm{T}}, \mathbf{q}_{\mathrm{T}}) = \sqrt{2(p_{\mathrm{T}} q_{\mathrm{T}} - \mathbf{p}_{\mathrm{T}} \cdot \mathbf{q}_{\mathrm{T}})}.$$

  In events with more than two τ-lepton candidates, only two leptons are used to compute m_{T2}. In such events m_{T2} is calculated for all pairs of leptons, and the pair that maximises m_{T2} is used to assign the m_{T2} value of the event. Similarly, in the intermediate Wh analysis, m_{T2} is calculated separately for each possible pairing of lepton-τ or τ-τ, and the maximum value is taken as the m_{T2} value for the event. For $t\bar{t}$ and WW events, in which two W bosons decay leptonically and $\mathbf{p}_{\mathrm{T}}^{\mathrm{miss}}$ is the sum of the transverse momenta of the two neutrinos, the m_{T2} distribution has a kinematic endpoint at the W boson mass. For large mass differences between the $\tilde{\chi}_1^{\pm}/\tilde{\chi}_2^0$ and the $\tilde{\chi}_1^0$, the m_{T2} distribution for signal events extends significantly beyond this endpoint. The $\tilde{\chi}_1^0$ is assumed to be massless in the calculation of m_{T2}.

- $m_{\mathrm{T},\ell}$, the transverse mass values obtained from the light lepton with the $E_{\mathrm{T}}^{\mathrm{miss}}$, where ℓ can be e or μ.

- m_{Tsum}, the sum of the transverse mass values of the leading and next-to-leading τ-lepton candidates with the $E_{\mathrm{T}}^{\mathrm{miss}}$ for $\tilde{\chi}_1^+\tilde{\chi}_1^-$ and $\tilde{\chi}_1^\pm\tilde{\chi}_2^0$ with decays to an intermediate stau channels. In the $\tilde{\chi}_1^\pm\tilde{\chi}_2^0$ with decays to an intermediate Wh scenario, m_{Tsum} also includes $m_{\mathrm{T}\ell}$.
- $\Delta R(\tau_1,\tau_2) = \sqrt{(\Delta\eta(\tau_1,\tau_2)^2 + \Delta\phi(\tau_1,\tau_2)^2}$, the angular distance between the leading and next-to-leading τ-lepton candidate. An upper cut on this variable is used to discriminate against back-to-back objects in SM events.
- $m(\tau_1,\tau_2)$: the invariant mass of the two reconstructed leading τ-lepton candidates.
- $|\Delta\phi(\tau_1,\tau_2)|$: the absolute value of the difference of azimuthal angle around the z-axis between the leading τ-lepton candidates.

6 Intermediate stau channel

The intermediate stau channel targets two different production mechanisms, $\tilde{\chi}_1^\pm\tilde{\chi}_2^0$ (C1N2) and $\tilde{\chi}_1^+\tilde{\chi}_1^-$ (C1C1), with decays to the lightest neutralino only through intermediate stau and tau sneutrinos. The C1N2 analysis is then sub-divided into final states where the two leading τ-lepton candidates have opposite sign (OS) charge (C1N2OS) or have same sign (SS) charge, denoted as (C1N2SS). The SRs are separated into low mass (LM) and high mass (HM) regions to target respectively low or high $\tilde{\chi}_1^\pm/\tilde{\chi}_2^0$ mass regions. The high mass regions target the reach beyond the partial Run-2 dataset from the ATLAS collaboration, and the low mass regions target sensitivity in smaller mass splittings. The event selections of C1C1, C1N2OS and C1N2SS analyses are described in Section 6.1, and the background estimations are described in Section 6.2.

6.1 Event selection

The SRs were optimized by varying the kinematic selection criteria resulting in six SRs defined to cover both LM and HM regions for C1C1, C1N2OS and C1N2SS channels. The SRs were optimised to obtain the best expected sensitivity against the SM backgrounds.

The events used in this channel are selected using either an asymmetric *di-*τ trigger or a combined *di-*τ + E_T^{miss} trigger. Events which pass the asymmetric di-τ trigger for 2015 - 2017 (2018) datasets are required to have a leading τ-lepton candidate which has $p_{\mathrm{T}} > 95$ GeV and a next-to-leading τ-lepton candidate with $p_{\mathrm{T}} > 60$ (75) GeV. Events which pass the di-τ + $E_{\mathrm{T}}^{\mathrm{miss}}$ trigger for 2015 - 2017 (2018) datasets are required to have a leading τ-lepton candidate with $p_{\mathrm{T}} > 50$ (75) GeV and a next-to-leading τ-lepton candidate with $p_{\mathrm{T}} > 40$ GeV. In events selected by the di-τ + $E_{\mathrm{T}}^{\mathrm{miss}}$ trigger, the reconstructed $E_{\mathrm{T}}^{\mathrm{miss}}$ must also be larger than 150 GeV.

For the C1N2OS (C1N2SS) channels, events are required to have at least two medium τ-lepton candidates with OS (SS), while for the C1C1 channel, events are required to have exactly two medium τ-lepton candidates with OS. In the LM signal regions, SR-C1C1-LM and SR-C1N2OS-LM, at least one of the τ-lepton candidates must satisfy a tighter identification criteria, denoted as a "tight" τ-lepton candidate [74] to suppress quark or gluon jets mis-identified as τ-leptons in the lower $E_{\mathrm{T}}^{\mathrm{miss}}$ region. Additionally, a cut of $E_{\mathrm{T}}^{\mathrm{miss}} > 60$ GeV is required in these two SRs to further suppress background from mis-identified τ-leptons.

To discriminate the SUSY signal events from SM background processes, additional requirements are applied to define the SR selections in final states with OS τ-leptons. For C1C1 and C1N2OS scenarios, the reconstructed invariant mass of the visible decay products of the two leading τ-lepton candidates, $m(\tau_1, \tau_2)$, must be larger than 120 GeV to remove τ-lepton candidates originating from decays of low-mass resonances and to suppress contributions from Z+jets and Higgs boson events (Z/h-veto).

To reject events from SM processes containing a top quark, selected events must not contain any b-tagged jets (b-jet veto). A lower bound on the m_{T2} is imposed to reduce contributions from $t\bar{t}$ and WW events, $m_{\mathrm{T2}} > 80$ GeV and $m_{\mathrm{T2}} > 85$ GeV, in SR-C1C1-LM and SR-C1C1-HM, respectively.

In addition, cuts on $|\Delta\phi(\tau_1, \tau_2)| > 1.5$ and $|\Delta\phi(\tau_1, \tau_2)| > 1.6$ in SR-C1C1-LM and SR-C1N2SS-LM, respectively, and jet multiplicity upper cuts are used to further suppress SM backgrounds and increase signal sensitivity for low mass SRs. Finally, the discriminating variables m_{T2}, and $m_{\mathrm{T}sum}$ are used to define the SRs.

The SR definitions are summarised in Table 1. To illustrate the SUSY signal in the VRs and SRs, reference points are chosen which are sensitive to the low mass and high mass SRs of the intermediate stau channels. These reference points are:

- $m(\tilde{\chi}_1^{\pm}, \tilde{\chi}_1^0) = (700, 400)$ GeV;
- $m(\tilde{\chi}_1^{\pm}/\tilde{\chi}_2^0, \tilde{\chi}_1^0) = (1100, 0)$ GeV;
- $m(\tilde{\chi}_1^{\pm}/\tilde{\chi}_2^0, \tilde{\chi}_1^0) = (157, 92)$ GeV;

Table 1: Summary of the selection requirements for the gaugino pair production SRs for channels that decay via an intermediate stau.

SR-C1C1-LM	SR-C1N2OS-LM	SR-C1N2SS-LM
= 2 medium τ (OS)	$\geq$ 2 medium τ (OS)	$\geq$ 2 medium τ (SS)
$\geq$ 1 tight τ		-
asymmetric di-τ Trigger		
$E_{\mathrm{T}}^{\mathrm{miss}} < 150$ GeV		
b-jet veto		
Z/h veto ($m(\tau_1, \tau_2) > 120$ GeV)		-
$\|\Delta\phi(\tau_1, \tau_2)\| > 1.6$	-	$\|\Delta\phi(\tau_1, \tau_2)\| > 1.5$
-	$N_{jets} < 3$	
$E_{\mathrm{T}}^{\mathrm{miss}} > 60$ GeV		$m_{\mathrm{Tsum}} > 200$ GeV
$m_{\mathrm{T2}} > 80$ GeV	$m_{\mathrm{T2}} > 70$ GeV	$m_{\mathrm{T2}} > 80$ GeV

SR-C1C1-HM	SR-C1N2OS-HM	SR-C1N2SS-HM
= 2 medium τ (OS)	$\geq$ 2 medium τ (OS)	$\geq$ 2 medium τ (SS)
di-τ + $E_{\mathrm{T}}^{\mathrm{miss}}$ Trigger		
$E_{\mathrm{T}}^{\mathrm{miss}} > 150$ GeV		
b-jet veto		
Z/h veto ($m(\tau_1, \tau_2) > 120$ GeV)		-
$m_{\mathrm{Tsum}} > 400$ GeV		$m_{\mathrm{Tsum}} > 450$ GeV
$m_{\mathrm{T2}} > 85$ GeV		$m_{\mathrm{T2}} > 80$ GeV

6.2 Background estimation

The main backgrounds contributing to the intermediate stau SRs are from multi-jet production with misidentified τ-leptons, W and Z boson production in association with jets, multi-boson production, and events containing a top quark, referred to as *top* background. Top background events originate mostly from $t\bar{t}$ production in association with additional jets or an additional W or Z boson.

Background events contain a combination of 'real' τ-leptons, defined as correctly identified τ-leptons, or 'misidentified' τ-leptons, which can originate from a mis-identified light-flavour quark or gluon jet, an electron, or a muon. Selected events from multi-jet production contain mostly misidentified τ-leptons originating from mis-identified jets The mis-identification probability is low, however multi-jet production has a large cross-section. The multi-jet contribution in the SRs is estimated from data, as described in Section 6.2.1.

The contribution of W+jets events, which contain one real τ-lepton from the W boson decay and one or more mis-identified jets, is estimated from MC simulation and normalised to data in a dedicated control region (CR), as described in Section 6.2.2. A dedicated CR is used to estimate the top backgrounds for the SS final state, where misidentified τ-lepton contributions are a dominant source, as described in Section 6.2.3.

Multi-boson production contributes mainly through events containing real τ-leptons resulting from WW and ZZ decaying into a $\tau\tau\nu\nu$ final state in C1C1 and C1N2OS scenarios, while in the C1N2SS scenario, the main process is WZ decaying into a $\tau\tau\tau\nu$ final state. The contribution from real τ-leptons exceeds 85-90% in Z+jets and diboson production. Additionally, the real τ-lepton contribution exceeds 80% in backgrounds containing top quarks in OS final states. These backgrounds are described in Section 6.2.4.

6.2.1 Multi-jet background estimation

The multi-jet background accounts for 28–48 % (<17 %) of the total SM yield in high mass SRs (low mass SRs) for all three scenarios. This contribution is estimated from data using the so-called *ABCD* method. All regions used for the ABCD method are schematically drawn in Figure 2. Four exclusive regions, labelled as A, B, C, and D, are defined in a two-dimensional plane as a function of two (or more) discriminating variables that are found to be approximately uncorrelated. Assuming the ratio of background events in the regions C and B is equal to that in the regions D and A, the number of events in region D, N_{D}, can be calculated from that in region A, N_{A}, multiplied by the transfer factor T = $N_{\mathrm{C}}/N_{\mathrm{B}}$. Region D corresponds to one of the SRs, whereas regions A, B, and C are control regions defined accordingly. In the following, regions A–D are labelled as CR-A, CR-B, CR-C, and SR-D. Furthermore, two validation regions, VR-E and VR-F, are defined corresponding to each SR. The validation regions are used to verify the reliability of the transfer factor obtained from the ABCD estimation and to estimate the systematic uncertainty from the residual correlation between the variables used to define the ABCD regions. All of the regions are defined to be orthogonal to one another.

A "very loose" τ-lepton identification criterion is used to define the regions CR-B, VR-E, and CR-A. The τ-lepton is also required to not pass the "medium" criterion to remain orthogonal to the requirements in SR-D. Additionally, the sign of the electric charge of the two τ-leptons (OS or SS), m_{T2} and $\mathrm{m_{Tsum}}$ are used to define control regions (CR-A, CR-B, and CR-C) and validation regions (VR-E and VR-F). In the C1C1 and C1N2OS scenarios, the m_{T2} variable is used to distinguish the regions of the ABCD method. In

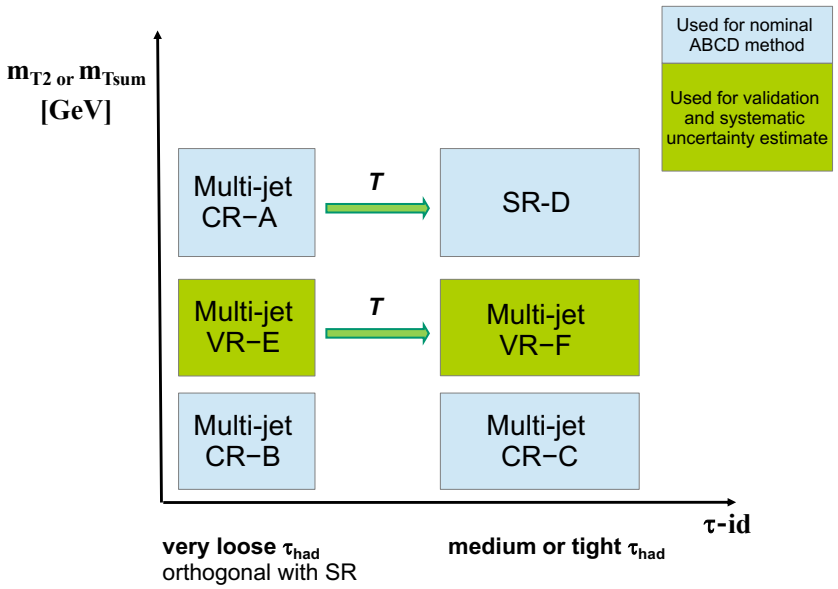

Figure 2: Illustration of the ABCD method for the multi-jet background determination. The control regions A, B, and C and signal region D are drawn as light blue boxes. Shown in green and labelled as VR are the regions E and F, which are used to validate the ABCD method and to estimate the systematic uncertainty.

the C1N2SS channel, m_{Tsum} is used to distinguish the various regions. The definition of the various ABCD regions can be found in Table 2.

Table 2: The definition of the ABCD regions for all channels in the intermediate stau scenario. Only those requirements that differ between the CRs/VRs and the SRs are listed. A "very loose" τ-lepton identification criterion is used to define the regions CR-B, VR-E, and CR-A. The τ-lepton is also required to not pass the "medium" criterion to remain orthogonal to the requirements in SR. The same τ-lepton identification criterion as that of the SR is used to define the regions CR-C and VR-F.

Channel	variable	CR-B / CR-C	VR-E / VR-F	CR-A / SR
C1C1-LM	m_{T2}	$\in$ [15, 35] GeV	$\in$ [35, 80] GeV	$>$ 80 GeV
	E_T^{miss}	$\in$ [10, 150] GeV	$\in$ [10, 150] GeV	$\in$ [60, 150] GeV
C1C1-HM	m_{T2}	$\in$ [35, 60] GeV	$\in$ [60, 85] GeV	$>$ 85 GeV
	m_{Tsum}	$\in$ [100, 300] GeV	$\in$ [200, 400] GeV	$>$ 400 GeV
	E_T^{miss}	$>$ 50 GeV	$>$ 50 GeV	$>$ 150 GeV
C1N2OS-LM	m_{T2}	$\in$ [15, 35] GeV	$\in$ [35, 70] GeV	$>$ 70 GeV
	E_T^{miss}	$\in$ [10, 150] GeV	$\in$ [10, 150] GeV	$\in$ [60, 150] GeV
C1N2OS-HM	m_{T2}	$\in$ [35, 60] GeV	$\in$ [60, 85] GeV	$>$ 85 GeV
	m_{Tsum}	$\in$ [150, 300] GeV	$\in$ [200, 400] GeV	$>$ 400 GeV
	E_T^{miss}	$>$ 50 GeV	$>$ 50 GeV	$>$ 150 GeV
C1N2SS-LM	m_{Tsum}	$<$ 100 GeV	$\in$ [100, 200] GeV	$>$ 200 GeV
	$\lvert\Delta\phi(\tau_1,\tau_2)\rvert$	$<$ 1.5	$<$ 1.5	$>$ 1.5
C1N2SS-HM	m_{Tsum}	$\in$ [100, 200] GeV	$\in$ [200, 450] GeV	$>$ 450 GeV
	E_T^{miss}	$>$ 50 GeV	$>$ 50 GeV	$>$ 150 GeV

In all validation regions and both sets of CR-B and CR-C, the events are required to pass a di-τ trigger instead of the di-τ + $E_{\mathrm{T}}^{\mathrm{miss}}$ trigger to increase the statistics from the lower $E_{\mathrm{T}}^{\mathrm{miss}}$ requirements. The offline $E_{\mathrm{T}}^{\mathrm{miss}} > 150$ GeV requirement is also removed. The di-τ trigger requires the identification of two hadronically decaying τ-lepton candidates with transverse momenta exceeding the same set of thresholds for the di-τ + $E_{\mathrm{T}}^{\mathrm{miss}}$ trigger, such that no bias on the τ-leptons is introduced.

The number of multi-jet events in the control and validation regions is estimated from data after subtraction of other SM contributions estimated from MC simulation. In CR-B and VR-E, more than 90 % of the events are from multi-jet production, whereas for CR-A (CR-C) the multi-jet contribution accounts for 41–95 % (26–54 %) events in the different SRs. In VR-F, the multi-jet purity is in the range of 36–59 %. Agreement between data and the estimated SM background is found for the m_{T2} and m_{Tsum} distributions in the validation regions, as shown in Figure 3. Several signal reference points targeting sensitivity to LM and HM SRs are also shown to highlight the potential signal contamination in the VRs. The correlation between the τ-lepton identification and the kinematic variables is verified by studying the variation of the transfer factor as a function of the kinematic variables m_{T2} and $m_{\mathrm{T}sum}$, and is found to be negligible.

The signal contamination in a certain region is defined as the ratio of the number of signal events to the sum of the number of signal events and SM background processes. The signal contamination in CR-A for all SRs is negligible for the gaugino mass range ($m(\tilde{\chi}_1^{\pm}/\tilde{\chi}_2^0) > 400$ GeV). Masses below this range have been previously excluded by the ATLAS Collaboration.

6.2.2 *W*+jets background estimation

The production of W+jets events with at least one mis-identified τ-lepton is an important background, accounting for 4–16 % of the expected SM background in the SRs of this analysis. In order to correct the misidentified τ-lepton MC modelling and reduce theoretical uncertainty from W+jets background, dedicated control regions WCR-OS and WCR-SS are used to normalise the W+jets MC estimate to data for the C1C1, C1N2OS and C1N2SS scenarios. W bosons decaying to $\mu\nu$ are used to select a pure WCR. Events are required to pass a single-muon trigger using the lowest unprescaled p_{T} thresholds [80]. Events containing exactly one isolated μ and one τ-lepton with OS (SS) are selected for C1C1 and C1N2OS (C1N2SS) scenarios. Both charged leptons are required to pass the object definitions described in Section 4 and have $p_{\mathrm{T}} > 40$ GeV for the μ and $p_{\mathrm{T}} > 50$ GeV for the τ-lepton.

The contribution from events with top quarks is suppressed by rejecting events containing b-tagged jets. A selection is applied to identify top background events in the OS final states; these events are labeled as "top-tagged". The contransverse mass variable [81], m_{CT}, is used to identify events that are kinematically compatible with $t\bar{t}$ pair production. Furthermore, top-tagged events must have at least two jets with $p_{\mathrm{T}} > 20$ GeV, and the scalar sum of the p_{T} of at least one combination of two jets and the two leptons in the event must exceed 100 GeV. Events passing the top-tagged selection are vetoed in the WCR-OS and WVR-OS regions to reduce the top backgrounds in these regions.

The contributions from Z+jets, top-quark and multi-boson production are reduced by requiring $m_{\mathrm{T},\mu} <$ 140 GeV ($m_{\mathrm{T},\mu} < 150$ GeV and $m_{\mathrm{T},\mu} + m_{\mathrm{T},\tau} > 80$ GeV) in WCR-OS and WVR-OS (WCR-SS and WVR-SS). In order to select events with kinematics very similar to the SR definition, events with a small amount of $E_{\mathrm{T}}^{\mathrm{miss}}$ are removed using a cut of $E_{\mathrm{T}}^{\mathrm{miss}} > 60$ (50) GeV for the W CR and VR in the OS (SS) channel. Events in the WCR are selected by requiring $40 < m_{\mathrm{T2}}(\tau,\mu) < 70$ GeV ($m_{\mathrm{T2}}(\tau,\mu) < 60$ GeV), while $m_{\mathrm{T2}}(\tau,\mu) > 70$ (60) GeV is used to validate the W+jets estimate (W validation region, WVR) for the OS (SS) channel. The definitions of the WCR and WVR are given in Table 3.

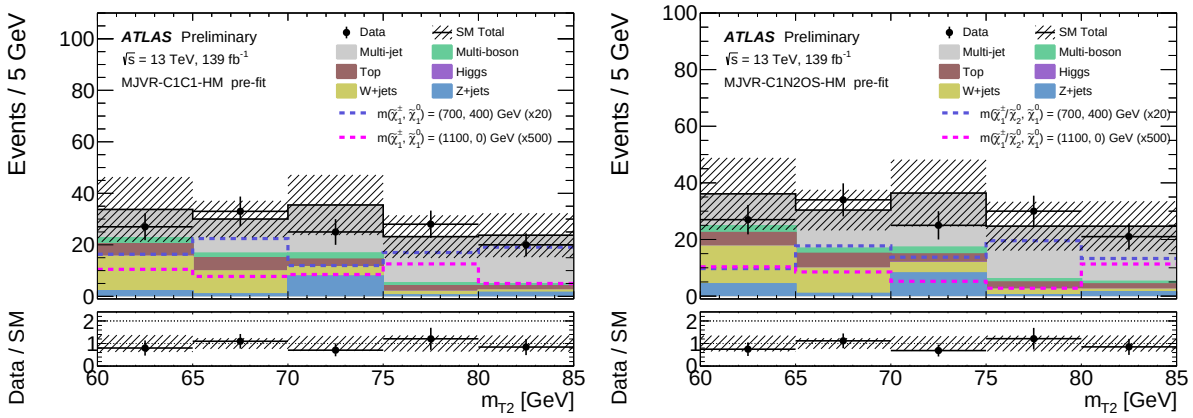

(a) (b)

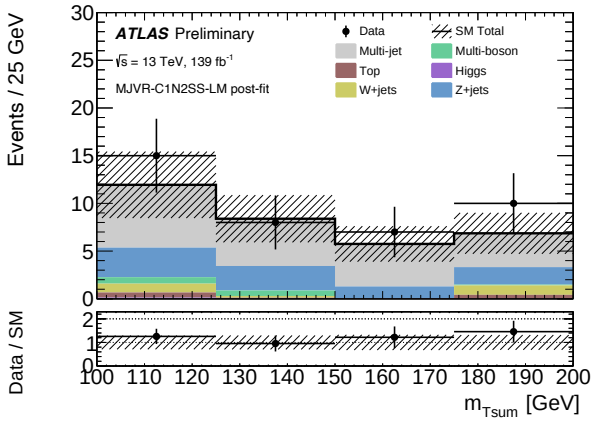

(c)

Figure 3: The post-fit kinematic distributions of m_{T2} and $m_{\mathrm{T}sum}$ in the multi-jet background VR-F for (a) SR-C1C1-HM (MJVR-C1C1-HM), (b) SR-C1N2OS-HM (MJVR-C1N2OS-HM) and (c) SR-C1N2SS-LM (MJVR-C1N2SS-LM), respectively. The stacked histograms show the contribution of the non-multi-jet SM backgrounds from MC simulation. The multi-jet contribution is estimated from data using the ABCD method. The hatched bands represent the combined statistical and systematic uncertainties in the sum of the SM backgrounds shown. For illustration, the distributions of the SUSY reference points are also shown as dashed lines in (a) and (b); figure (c) has no signal contamination. They are scaled by an additional factor to show the shape in the VRs. The lower panels show the ratio of data to the total SM background estimate.

Table 3: The definition of the W+jets control (WCR) and validation region (WVR).

WCR-OS	WVR-OS	WCR-SS	WVR-SS
baseline electron veto			
b-jet veto			
$p_{\mathrm{T}\tau} > 50$ GeV, $p_{\mathrm{T}\mu} > 40$ GeV			
= 1 medium τ, = 1 isolated μ (OS)		= 1 medium τ, = 1 isolated μ (SS)	
Top-tagged events veto		-	
$m_{\mathrm{T},\mu} < 140$ GeV		$50 < m_{\mathrm{T},\mu} < 150$ GeV	
-		$m_{\mathrm{T},\mu} + m_{\mathrm{T},\tau} > 80$ GeV	
$E_{\mathrm{T}}^{\mathrm{miss}} > 60$ GeV		$E_{\mathrm{T}}^{\mathrm{miss}} > 50$ GeV	
$40 < m_{\mathrm{T2}}(\tau,\mu) < 70$ GeV	$m_{\mathrm{T2}}(\tau,\mu) > 70$ GeV	$m_{\mathrm{T2}}(\tau,\mu) < 60$ GeV	$m_{\mathrm{T2}}(\tau,\mu) > 60$ GeV

The multi-jet contribution in the WCR (WVR) is estimated using the so-called OS–SS method by counting the number of events in data satisfying the same requirements as the WCR (WVR) but requiring the electric charge of the two leptons to be different from that in the SRs. Event yields from SM processes other than multi-jet production are subtracted from the data in the WCR, leaving only the events for the multi-jet estimate. The OS–SS method relies on the fact that in the multi-jet background, the ratio of SS to OS events is close to unity, while a significant difference from unity is expected for W+jets production. The latter is dominated by gu/gd-initiated processes that often give rise to a jet originating from a quark, the charge of which is anti-correlated with the W-boson charge. Based on studies with simulated samples, a conservative systematic uncertainty of 100 % is assigned to the estimate of the multi-jet event yield in the WCR.

The m_{T2} distribution in the WCRs is shown in Figure 4. The purity of the selection in W+jets events is 73–85 % in all W control and validation regions. The signal contamination in the WCR and WVR is negligible due to the additional μ requirement.

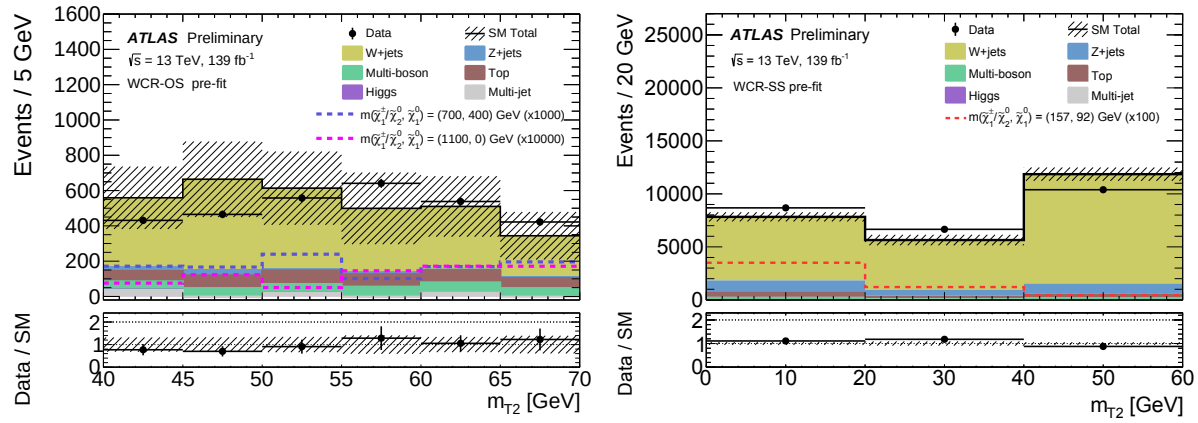

(a) (b)

Figure 4: The figure shows the pre-fit m_{T2} distribution for WCR used for the (a) C1C1, C1N2OS and (b) C1N2SS scenarios. The SM backgrounds other than multi-jet production are estimated from MC simulation. The multi-jet contribution is estimated from data using the *OS–SS* method for WCR. The hashed bands represent the combined statistical and systematic uncertainties of the total SM background. For illustration, the distributions of the SUSY reference points are also shown as dashed lines. The lower panels show the ratio of data to the total SM background estimate.

6.2.3 Top background estimation for C1N2SS

The top background is a dominant contribution in SR-C1N2SS-HM, which consists mainly of one or two misidentified τ-leptons from $t\bar{t}$ and Wt production. To estimate this background in SR-C1N2SS-HM, a data-driven approach is used to normalise the top background MC simulation to data using a dedicated top-enriched CR (TCR-SS-HM) and validated in a top-enriched VR (TVR-SS-HM), described in Table 4. To increase the statistics, the τ-lepton identification working point was loosened. The requirement of $E_{\mathrm{T}}^{\mathrm{miss}} > 150$ GeV is applied to reduce the contribution of multi-jet processes in TVR-SS-HM. The top background in SR-C1N2SS-LM is estimated with MC simulation directly given it has a negligible contribution (<1%), which mainly arises from the Zt process from two real τ-leptons. The top background purity is found to be more than 83% in TCR-SS-HM and TVR-SS-HM. The visible mass spectrum of the two τ-leptons, $\mathrm{m_{vis}}(\tau_1,\tau_2)$, in TCR-SS and TVR-SS-HM is shown in Figure 5. The signal contamination is significantly reduced due to the b-jet requirement. The top background, mainly driven by the mis-identified τ-leptons, is found to be overestimated in TCR-SS-HM and can be seen in Figure 5 (a). The visible mass spectrum is also shown after the fit to data in TVR-SS-HM in Figure 5 (b), where good agreement with data can be seen close to the SR.

Table 4: The definition of the top control (TCR) and validation region (TVR) for C1N2SS.

TCR-SS-HM	TVR-SS-HM
2 τ channel	
Di-τ + $E_{\mathrm{T}}^{\mathrm{miss}}$ trigger	
≥ 2 very loose τ, ≥ 1 loose τ	
$N_{\text{medium-}\tau} < 2$	
≥ 1 b-jet	
$E_{\mathrm{T}}^{\mathrm{miss}} > 150$ GeV	
$m_{\mathrm{Tsum}} \leq 400$ GeV	$m_{\mathrm{Tsum}} \geq 400$ GeV

6.2.4 Irreducible background estimation

Additional irreducible SM backgrounds are estimated from MC simulation and checked in dedicated VRs. The top background contribution in OS final states are small and amounts to about 7–14 % of the total background in all SRs. The MC estimates are validated in regions enriched in top-quark events. TVR-OS-LM (TVR-OS-HM) has been defined to validate the top background in the low (high) mass SRs. At least two medium τ-leptons are required, in which at least one τ-lepton candidate must satisfy the tight τ-lepton identification criteria. To be orthogonal with the SRs and increase the contribution from top events, one b-tagged jet with $p_{\mathrm{T}} > 20$ GeV is required. $|\Delta\phi(\tau_1,\tau_2)| > 1.0$ and $E_{\mathrm{T}}^{\mathrm{miss}} > 20$ GeV are used to suppress the Z+jets background. $m(\tau_1,\tau_2) > 120$ GeV is required to additionally suppress Z+jets and Higgs boson backgrounds, while remaining orthogonal to the SR. To further suppress other SM background contributions, $m_{\mathrm{Tsum}} > 150$ GeV and $\mathrm{m_{T2}} > 40$ (30) GeV selections are required in TVR-OS-LM (TVR-OS-HM).

Furthermore in OS final states, the Z+jets contribution is around 16–21 % of the total background in all SRs, which mainly arises from $Z \rightarrow \tau\tau$ decays. The multi-boson background accounts for 25–50 % of the total SM contribution in the SRs and mainly arises from $WW \rightarrow \tau\nu\tau\nu$ and $ZZ \rightarrow \tau\tau\nu\nu$ events. The purity of real τ-leptons is higher than 96 %.

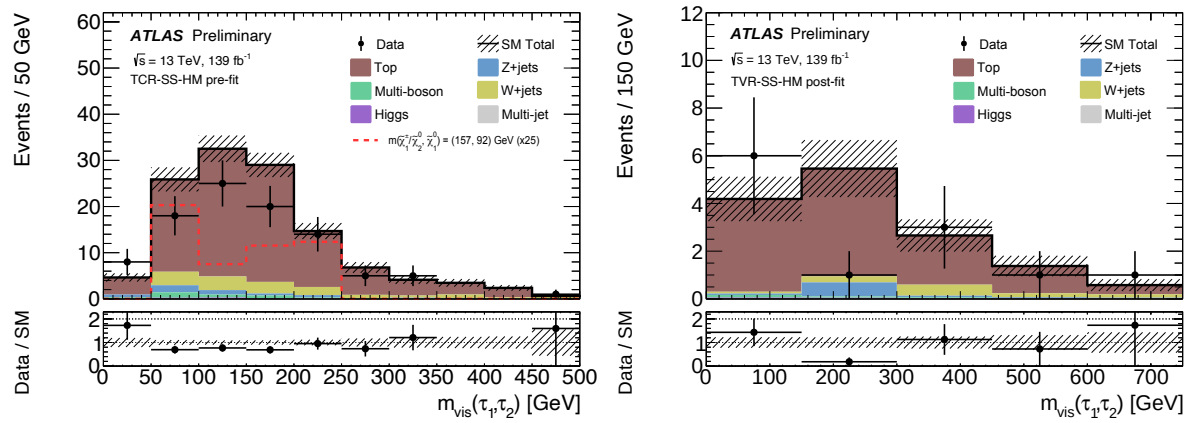

(a) (b)

Figure 5: The pre-fit (a) and post-fit (b) $m_{\text{vis}}(\tau_1,\tau_2)$ distribution in the TCR-SS-HM and TVR-SS-HM, respectively. The other SM backgrounds are estimated from MC simulation. The hashed bands represent the combined statistical and systematic uncertainties of the total SM background. For illustration, the distributions of the SUSY reference point scaled by a factor of 25 is also shown as dashed lines. The lower panel shows the ratio of data to the total SM background estimate. The last bin in both plots includes the overflow events.

To validate the MC modelling and normalisation of the Z+jets and multi-boson processes, four dedicated VRs are defined. ZVR-OS-LM (MBVR-OS-LM) is defined to validate Z+jets (multi-boson) MC modelling in the low mass SRs, while ZVR-OS-HM (MBVR-OS-HM) is defined to validate the MC modelling in the high mass SRs. At least two τ-lepton candidates must satisfy the medium τ-lepton identification criteria. To suppress top-quark backgrounds, events containing b-jets are vetoed and a lowered $E_{\text{T}}^{\text{miss}}$ threshold of 40 (70) GeV has been used in ZVR-OS-LM (MBVR-OS-LM). Upper cuts on $|\Delta R(\tau_1,\tau_2)| < 1.0$ ($|\Delta R(\tau_1,\tau_2)| < 1.2$ and $|\Delta\phi(\tau_1,\tau_2)| < 1.0$) is used to suppress other SM backgrounds in Z+jets (multi-boson) VRs. In the MBVRs, $m_{\text{T},\tau 1} + m_{\text{T},\tau 2} > 180$ GeV is also required to enrich the multi-boson contribution and suppress the Z+jets events. Finally, the ZVRs and MBVRs are separated by an m_{T2} cut at 60 GeV to keep them orthogonal and further increase their purity.

The purity of the selection in Z+jets and $t\bar{t}$ events is in the range of 81–99 % in the respective validation regions, and the purity of the selection in multi-boson events is around 41–68 % in the MBVRs. The signal contamination in the above VRs is small due to the b-jet requirement in the top VRs and the $m(\tau_1,\tau_2)$ upper cuts in the Z+jets and multi-boson VRs.

In the SS final state, the multi-boson background is estimated from MC simulation and validated in a dedicated VR (MBVR-SS). The region contains two isolated muons with OS. Events are required to pass the single muon trigger requirement. The events with b-tagged jets have been vetoed to suppress top contribution. To enrich multi-boson production a $|\Delta\phi(\tau, E_T^{\text{miss}})| < 1.75$ cut has been applied. Finally, a looser $E_{\text{T}}^{\text{miss}}$ cut of 100 GeV has been required to further improve multi-boson purity. The multi-boson purity is found to be 73%.

The agreement between data and the SM prediction is shown in all validation and signal regions for the intermediate stau channels in Figure 6 after the background-only fit to data has been applied, as described in Section 9.1.

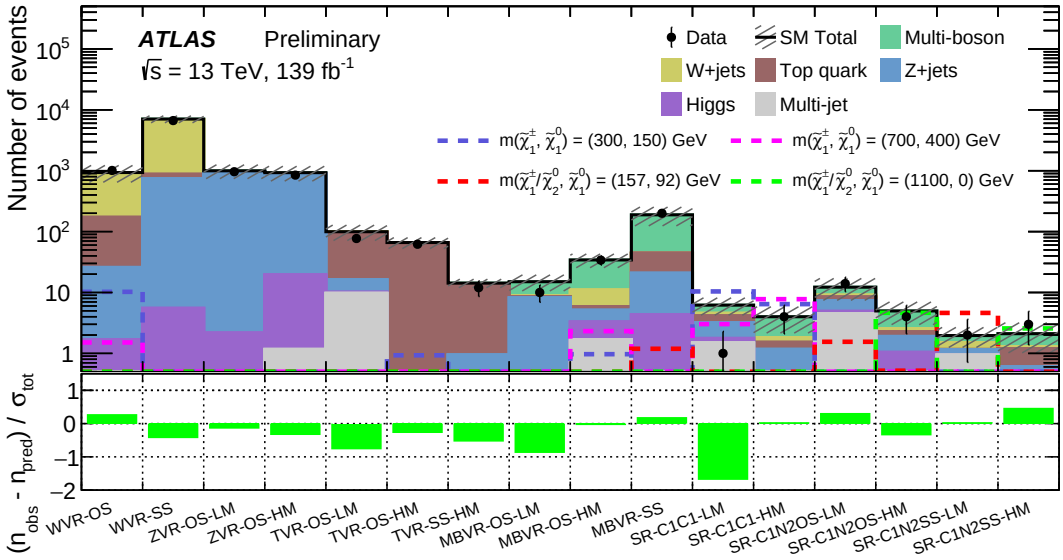

Figure 6: Comparison of the observed and expected event yields in all VRs and SRs in the background-only fit. The SM backgrounds other than multi-jet production are estimated from MC simulation. The multi-jet contribution is negligible and is estimated from data using the ABCD method. The hatched bands represent the combined statistical and systematic uncertainties of the total SM background. The background-only fit to data is used, described in Section 9.1. For illustration, the distributions from the SUSY reference points are also shown as dashed lines.

7 Intermediate Wh channel

The search for the production of $\tilde{\chi}_1^{\pm}\tilde{\chi}_2^0$ decaying via an intermediate W and h boson (Wh analysis) is described in this section. The event selection of the intermediate Wh channel is described in Section 7.1 and the background estimations are described in Section 7.2.

7.1 Event selection

The selected events are required to pass the lowest unprescaled light lepton trigger. The selected light-lepton (e or μ) must pass the signal electron or muon requirements described in Section 4.

Two SRs are defined to cover low (SR-Wh-LM) and high (SR-Wh-HM) gaugino mass regions. The two SRs are not orthogonal due to limitations from the available statistics in the dataset. Events are required to have exactly one e or μ and at least two medium τ-lepton candidates with opposite sign for the first two leading τ-leptons. An additional requirement of $|\Delta\phi(\tau_1, \tau_2)| < 3$ has been applied to avoid back-to-back τ-lepton events. The invariant mass of the two visible leading τ-lepton candidates ($m(\tau_1, \tau_2)$) is required to be in the Higgs mass window of [90, 130] GeV in the SR-Wh-LM regions and [80, 160] GeV in the SR-Wh-HM region. This requirement also suppresses other SM backgrounds from top and W+jets. To reject events from SM processes containing a top quark, selected events must not contain any b-tagged jets

(b-jet veto). The requirement of $|\Delta R(\tau_1, \tau_2)| < 2.2$ is applied to suppress fake τ-lepton contribution from top backgrounds in SR-Wh-HM. To discriminate the SUSY signal events from SM background processes, additional requirements on the discriminating variable $m_{\mathrm{T2}} > 100$ (80) GeV are applied in SR-Wh-LM (SR-Wh-HM). To further suppress SM background and improve signal sensitivity in the SR-Wh-HM, $m_{\mathrm{T},\ell} > 80$ GeV and $m_{\mathrm{T}sum} > 450$ GeV requirements are also applied. The requirements for the two SRs are summarised in Table 5. For representation in the intermediate Wh channel, a SUSY reference point has been chosen for a simplified model for $\tilde{\chi}_1^{\pm}\tilde{\chi}_2^0$ production via Wh decay with the masses of the $\tilde{\chi}_1^{\pm}$ and the $\tilde{\chi}_2^0$ equal to 225 GeV, and $\tilde{\chi}_1^0$ mass equal to 75 GeV.

Table 5: Summary of selection requirements for the SRs of gaugino pair production decaying to an intermediate Wh for low mass and high mass regions. The two SRs are not orthogonal.

SR-Wh-LM	SR-Wh-HM
= 1 light lepton	
≥ 2 medium τ (OS)	
b-jet veto	
$\lvert\Delta\phi(\tau_1, \tau_2)\rvert < 3$	
-	$\Delta\mathrm{R}(\tau_1, \tau_2) < 2.2$
$90 < m(\tau_1, \tau_2) < 130$ GeV	$80 < m(\tau_1, \tau_2) < 160$ GeV
$m_{\mathrm{T2}} > 100$ GeV	$m_{\mathrm{T2}} > 80$ GeV
-	$m_{\mathrm{T},\ell} > 80$ GeV
-	$m_{\mathrm{T}sum} > 450$ GeV

7.2 Background estimation

The final state is characterised by the presence of two hadronically decaying τ-lepton candidates from the Higgs boson decay and one light lepton from W-boson decay. The backgrounds can be categorised into two groups. The first group includes events with a light lepton and two real τ-leptons. This category is dominated by multi-boson events. A small contribution is expected from other SM processes such as $t\bar{t}$, Wt and Z+jets. The second group includes events with one or two misidentified τ-leptons from mis-identified jets. Events with two misidentified τ-leptons are mostly from W+jets events and are estimated using a data-driven technique. Events with a single misidentified τ-lepton are dominated by events with a top quark, with smaller contributions from Z+jets and multi-boson. Overall, the dominant background contributions in both SRs are from top and multi-boson processes, and account for 89–90% of the total.

Events with two misidentified τ-leptons are modelled with the fake factor method described in Section 7.2.1. A dedicated CR and VR are used to estimate and validate the data-driven measurement of this background, respectively. Top backgrounds are estimated using a dedicated CR described in Section 7.2.2. A VR is used to validate the multi-boson background which is estimated directly from MC simulation as discussed in Section 7.2.3. All other SM backgrounds are estimated directly from MC simulation.

7.2.1 Misidentified τ-lepton background estimation

The fake factor method uses a control data sample (FF CR) with only τ-lepton candidates that fail the baseline τ-lepton identification requirement to estimate events with two misidentified τ-leptons. This

estimate is obtained as the product of the number of events and the fake factor, which relates the number of events with looser tau-lepton candidates to the number where tau leptons meet the nominal identification criteria.

To compute the fake factor (FF), a looser set of criteria for the tau identification is used, providing a selection orthogonal to the default τ-lepton selection. The control sample is referred to as the anti-τ-lepton sample. The FF value for each of the τ-lepton candidates is the ratio of the number of events with a τ-lepton passing the identification requirements to the number passing the anti-tau selection requirements. To estimate the two misidentified τ-lepton contributions, three control regions are defined: a region where both the leading and sub-leading p_{T} τ-lepton candidate satisfy the anti-tau criteria ("AA" region), the region where the leading τ-lepton candidate passes the medium τ-lepton identification criteria and the sub-leading τ-lepton candidate satisfies the anti-tau criteria ("MA" region), and a region where both leading and sub-leading τ-lepton candidate pass the medium τ-lepton identification criteria ("MM" region). In this case, the fake factor extrapolation to the SR is derived for the leading τ-lepton candidate first, then the sub-leading τ-lepton candidate.

The estimation of the total contribution from two misidentified τ-leptons (N_{fakes}) can be written as the product of the two fake factors ($\mathrm{FF}^{\mathrm{CR}}_{\tau i}$) and the number of events from the "AA" region ($N_{\mathrm{AA,\ fake\ bkg}}$):

$$N_{\mathrm{fakes}} = N_{\mathrm{AA,\ fakes}} \times \mathrm{FF}^{\mathrm{CR}}_{\tau 1} \times \mathrm{FF}^{\mathrm{CR}}_{\tau 2}, \tag{1}$$

where the individual fake factors for the two τ-leptons are written as:

$$\mathrm{FF}^{\mathrm{CR}}_{\tau 1} = \frac{N_{\mathrm{data,AA}} - N^{\geq 1\ \mathrm{truth}\ \tau}_{\mathrm{MC,AA}}}{N_{\mathrm{data,MA}} - N^{\geq 1\ \mathrm{truth}\ \tau}_{\mathrm{MC,MA}}} \tag{2}$$

$$\mathrm{FF}^{\mathrm{CR}}_{\tau 2} = \frac{N_{\mathrm{data,MA}} - N^{\geq 1\ \mathrm{truth}\ \tau}_{\mathrm{MC,MA}}}{N_{\mathrm{data,MM}} - N^{\geq 1\ \mathrm{truth}\ \tau}_{\mathrm{MC,MM}}} \tag{3}$$

The contamination from events with at least one real τ-lepton ($N^{\geq 1\ \mathrm{truth\ tau}}_{\mathrm{MC}}$) is estimated from simulation and subtracted when calculating the ratio.

The fake factors are calculated in a W-enriched control region (FFCR-Wh). Top contribution from non-W+jets backgrounds with two misidentified τ leptons is less than 6–7 %, and is included in the estimation from the fake factor method. A loose FFCR-Wh has been defined to increase the statistics in the control region by inverting the OS requirement to be orthogonal with the SR and using looser kinematic selection cuts. The selection criteria are summarised in Table 6.

Table 6: The definition of the fake factor control and validation regions, FFCR-Wh and FFVR-Wh, respectively.

FFCR-Wh	FFVR-Wh
≥ 2 very loose τ (SS)	≥ 2 medium τ (OS)
$m(\tau_1, \tau_2) > 20$ GeV	$40 < m(\tau_1, \tau_2) < 160$ GeV
$m_{\mathrm{T2}} > 20$ GeV	$m_{\mathrm{T2}} > 30$ GeV
b-jet veto	
$\lvert\Delta\phi(\tau_1, \tau_2)\rvert < 3$	
=1 light lepton (e or μ)	

The fake factor dependencies on the parameters of the hadronically decaying τ-lepton candidate, such as the number of tracks, transverse momentum p_T and $|\eta|$, have been studied and found to be minimal for all parameters except the number of tracks (1-prong or 3-prong τ-leptons). The fake factors are measured in bins of p_T and $|\eta|$, separately for 1-prong and 3-prong τ-leptons. The binning has been optimized based on the available statistics. The fake factor for leading and subleading τ-lepton is similar and found to be around 0.4 (0.1) for the 1-prong (3-prong) τ-lepton. The fake factor estimation has been validated in a misidentified τ-lepton dominated VR (FFVR-Wh) with a selection similar to the SR-Wh-LM with selection criteria on $m(\tau_1, \tau_2)$ and m_{T2}, as shown in Table 6. The kinematic distributions in FFVR-Wh are shown in Figure 7 and good agreement between data and SM prediction is observed.

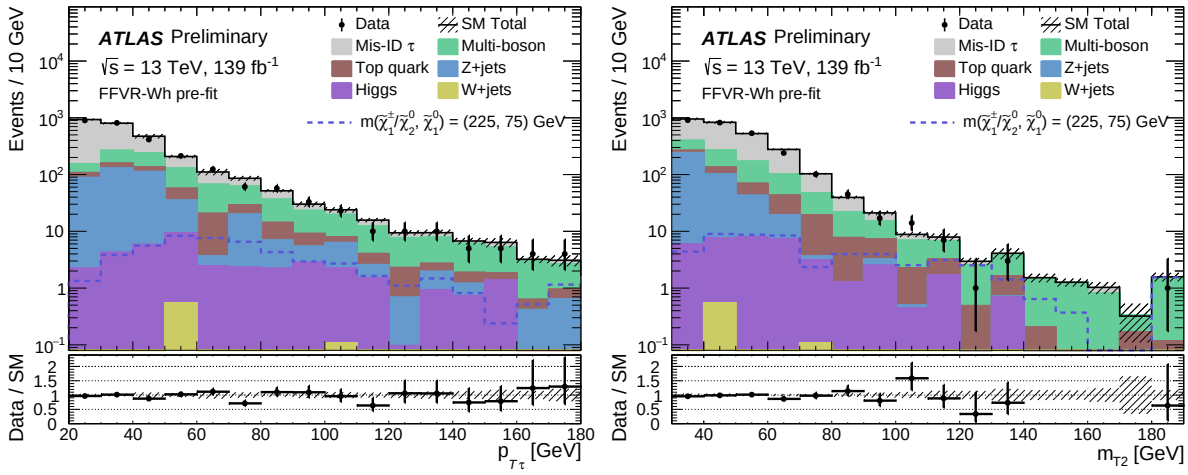

(a) (b)

Figure 7: The distribution of the leading τ-lepton transverse momentum ($\mathrm{p_{T\tau}}$) (a) and m_{T2} (b) variables in the FFVR-Wh. The SM backgrounds other than the misidentified τ-lepton contribution are estimated from MC simulation. The misidentified contribution with at least two misidentified τ-leptons (Mis-ID τ) is estimated from data using the fake factor method. The hatched bands represent the combined statistical and systematic uncertainties of the total SM background. For illustration, the distributions of the SUSY reference points are also shown as dashed lines. The lower panels show the ratio of data to the total SM background estimate. The last bin in both plots includes the overflow events.

7.2.2 Top background estimation

The top background is a sub-dominant contribution in the SR-Wh-LM. It is comprised mainly of $t\bar{t}$ events with one W-boson decay to an electron or muon, and the other to a τ-lepton. The second τ-lepton typically originates from a mis-identified jet. In the SR-Wh-HM, the top contribution is negligible and largely the result of two misidentified τ-leptons. The two misidentified τ-lepton contribution is accounted for in the estimation with the FF method.

The top background MC estimate, including final states with events with one misidentified τ-lepton, is estimated from MC and normalized to data using a top enriched control region (TCR-Wh). This estimation is validated in a Top VR (TVR-Wh). The TCR and TVR are defined in a similar manner as the SR except for the b-jet veto, replaced by a $1 \leq N_{b-\mathrm{jets}} \leq 2$ requirement. The TCR and TVR regions are split by the m_{T2} variable at a value of 80 GeV. To increase the statistics, the OS requirement is removed and $m(\tau_1, \tau_2)$ requirement is also loosened to $40 < m(\tau_1, \tau_2) < 160$ GeV in the TCR-Wh and TVR-Wh. To further

improve the purity of the top background, a cut on $m_{\mathrm{T}sum} > 250$ GeV is used. The summary of the TCR and TVR are shown in Table 7. The top background composition determined from MC is found to be similar across the CR, VR and SR. The m_{T2} distribution in the TCR and TVR is shown in Figure 8. Good agreement between data and SM in both the top CR and VR is observed. The top purity is between 73–81% in the CR and VR.

Table 7: The definition of the top control and validation regions for the intermediate Wh channel.

TCR-Wh	TVR-Wh
=1 light lepton (e or μ)	
≥ 2 medium τ	
$40 < m(\tau_1, \tau_2) < 160$ GeV	
$m_{\mathrm{T}sum} > 250$ GeV	
$1 \leq N_{b-\mathrm{jets}} \leq 2$	
$\lvert\Delta\phi(\tau_1, \tau_2)\rvert < 3$	
20 GeV $< m_{\mathrm{T2}} <$ 80 GeV	$m_{\mathrm{T2}} > 80$ GeV

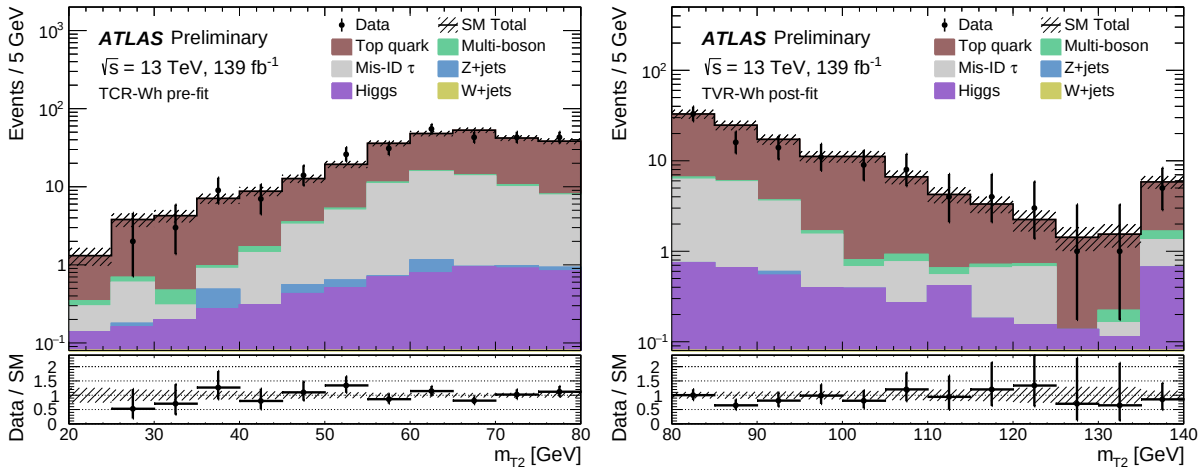

(a) (b)

Figure 8: The pre-fit (post-fit) m_{T2} distribution in the TCR-Wh (a) (TVR-Wh (b)). The SM backgrounds other than misidentified contribution are estimated from MC simulation. The misidentified contribution with at least two misidentified τ-leptons (Mis-ID τ) is estimated from data using the FF method. The hatched bands represent the combined statistical and systematic uncertainties of the total SM background. The lower panels show the ratio of data to the total SM background estimate. The last bin in figure (b) includes the overflow events.

7.2.3 Multi-boson background estimation

Multi-boson production is the dominant SM contribution in both SRs. The main contribution is WZ production decaying to $lll\nu$ with one light lepton and two real τ-leptons in both SRs. Additional smaller contributions in SR-Wh-LM stem from ZZ or WW production decaying to $ll\nu\nu$ with one real τ-lepton and one misidentified τ-lepton.

The multi-boson background is estimated from MC simulation and validated in a multi-boson enriched region (MBVR-Wh). A lower $m(\tau_1, \tau_2)$ window $40 < m(\tau_1, \tau_2) < 70$ GeV and an upper m_{T2} cut of 80 GeV are required, such that the MBVR-Wh is orthogonal to the SRs. To suppress the W+jets and Z+jets backgrounds and increase the multi-boson purity, a cut of $p_{\mathrm{T}\tau_2} > 30$ GeV is applied. To further suppress the Z+jets background, $m_{\mathrm{T},l} > 70$ GeV is required. The definition of the MBVR-Wh is shown in Table 8. The post-fit m_{T2} distribution in the MBVR is shown in Figure 9. Good agreement between data and SM in the multi-boson VR is observed. The multi-boson purity is found to be 61% in MBVR-Wh.

Table 8: The definition of the multi-boson validation region (MBVR-Wh).

MBVR-Wh
= 1 light lepton (e or μ)
$\geq$ 2 medium τ (OS)
$40 < m(\tau_1, \tau_2) < 70$ GeV
$p_{T\,\tau_2} > 30$ GeV
$m_{\mathrm{T},l} > 70$ GeV
$m_{\mathrm{T2}} < 80$ GeV
b-jet veto
$\lvert\Delta\phi(\tau_1, \tau_2)\rvert < 3$

The agreement between data and the SM prediction is shown in the validation and signal regions for the intermediate Wh channels in Figure 10 after the background-only fit to data has been applied, as described in Section 9.1. The signal reference point for $\tilde{\chi}_1^{\pm}\tilde{\chi}_2^0$ production via Wh decay with the masses of the $\tilde{\chi}_1^{\pm}$ and the $\tilde{\chi}_2^0$ equal to 225 GeV, and $\tilde{\chi}_1^0$ mass equal to 75 GeV is shown in the figure.

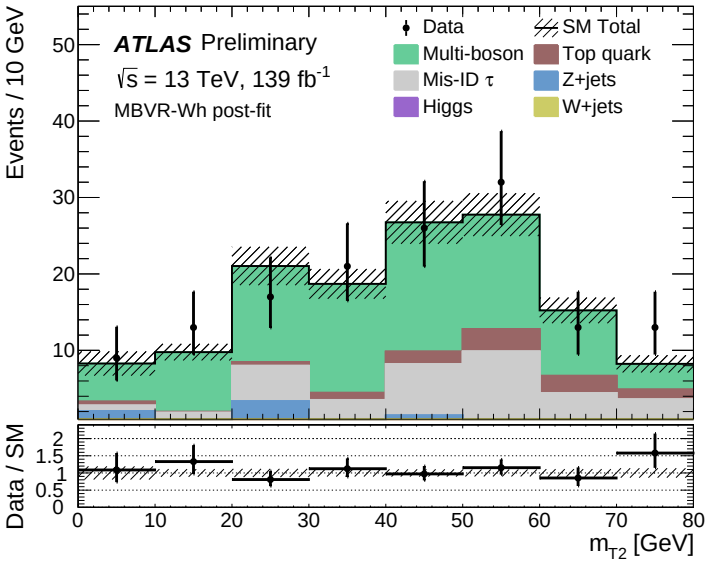

Figure 9: The post-fit m_{T2} distribution in the MBVR-Wh. The SM backgrounds other than misidentified contribution are estimated from MC simulation. The misidentified contribution with at least two misidentified τ-leptons (Mis-ID τ) is estimated from data using the FF method. The hatched bands represent the combined statistical and systematic uncertainties of the total SM background. The lower panels show the ratio of data to the total SM background estimate. The last bin includes the overflow events.

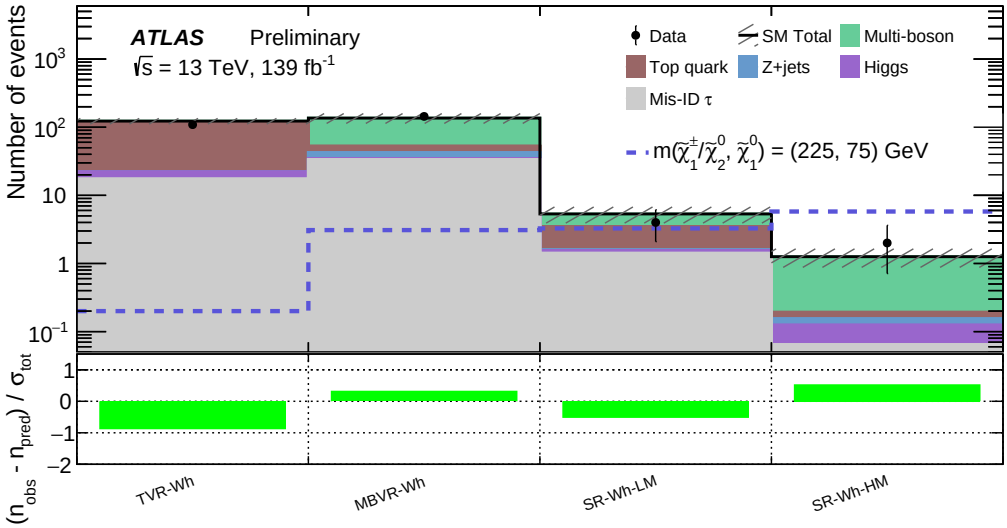

Figure 10: Comparison of the observed and expected event yields in the TVRs and MBVRs as well as two SRs in the background-only fit. The SM backgrounds other than multi-jet production are estimated from MC simulation. The misidentified contribution (Mis-ID τ) is estimated from data using the FF method. The hatched bands represent the combined statistical and systematic uncertainties of the total SM background. The background-only fit to data is used, as described in Section 9.1. For illustration, the expectation of the SUSY reference point mass of $(\tilde{\chi}_1^{\pm}/\tilde{\chi}_2^0,\tilde{\chi}_1^0)$ = (225,75) GeV is also shown as a dashed line.

8 Systematic uncertainties

Systematic uncertainties have an impact on the estimates of the background and signal event yields in the control and signal regions. Uncertainties arising from experimental effects and theoretical sources are estimated. The main sources of experimental systematic uncertainty in the SM background estimates include τ-lepton and jet-energy calibrations and resolution, τ-lepton identification, systematic effects due to the presence of pile-up events, and uncertainties related to the modelling of $E_{\mathrm{T}}^{\mathrm{miss}}$ in the simulation. The uncertainties in the energy and momentum scale of each of the objects entering the $E_{\mathrm{T}}^{\mathrm{miss}}$ calculation are estimated, as well as the uncertainties in the soft-term resolution and scale [82]. A variation in the pile-up reweighting of the MC simulated event samples is included to cover the uncertainty in the ratio of the predicted and measured inelastic cross-section [83].

Theoretical uncertainties affecting the main reducible backgrounds are estimated by varying the generator parameters: renormalisation and factorisation scale as well as PDF uncertainties following the PDF4LHC recommendations [84]. Uncertainties due to the choice of renormalisation and factorisation scales are included by varying the scales from their nominal values by a factor of two or one half. Additionally, cross-section uncertainties are assigned to be included in the normalisation of the signal and background processes.

Several sources of uncertainty are considered for the ABCD method used to determine the multi-jet

background estimation, they include: the correlation between the τ-lepton identification and the kinematic variables m_{T2}, the limited number of events in the CRs, and the subtraction of other SM backgrounds. The systematic uncertainty in the correlation is estimated by comparing the transfer factor from CR-B to CR-C to that of VR-E to VR-F. The systematic uncertainty in the non-multi-jet background subtraction in the control regions is estimated by considering the total uncertainties of the MC estimates of the non-multi-jet background in the CRs. The systematic uncertainty due to the limited number of events in the control regions is estimated by taking the statistical uncertainty of the event yields in these control regions.

Sources of uncertainty are considered for the fake factor method used to determine the misidentified background with at least two misidentified τ-leptons. The fake factor values are varied up and down by their statistical uncertainties and the difference is used as a source of uncertainty. A further 30% systematic uncertainty on the subtracted MC processes is used as a conservative estimation on the systematic uncertainty from MC subtractions in the FFCR-Wh. Additionally, the difference in the quark/gluon contributions in the fake factor control regions and signal regions are considered as additional uncertainties. The systematic uncertainties and their impact on each SR is summarised in Figure 11.

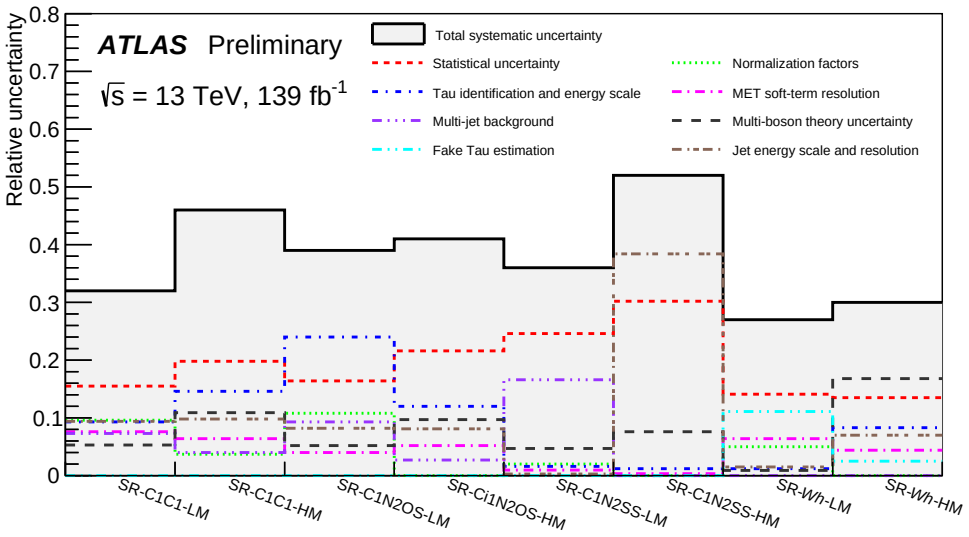

Figure 11: Summary of the total uncertainty on the predictions of the background event yields of each SR in all scenarios. The dominant systematic contributions are indicated by individual dashed lines. The total uncertainty in each SR is denoted by the solid black line.

The dominant contribution of systematic uncertainties in all scenarios are mainly from the statistics of the MC samples, the normalisation uncertainties of the multi-jet background, the τ-lepton identification and the energy scale, jet energy scale and resolution. In the intermediate stau channel, uncertainties on the multi-jet estimation also contribute. In the intermediate Wh channel, multi-boson cross-section uncertainties represent a major contribution to the systematics.

9 Results

9.1 Statistical analysis

The observed number of events in the CRs and SRs are used in a combined profile likelihood fit to determine the expected SM background yields. The statistical interpretation of the results is performed using the profile likelihood method implemented in the HistFitter framework [85]. Systematic uncertainties are included as nuisance parameters in the likelihood fits and are assumed to follow a Gaussian distribution with a width determined from the size of the uncertainty. Correlations of systematic uncertainties between control and signal regions, and between background processes are taken into account with common nuisance parameters. The fit parameters are determined by maximising the product of the Poisson probability functions and the constraints for the nuisance parameters. Three types of fit configurations are used to derive the results.

- The *background-only* fit uses as input the number of observed events in the CRs, the expected SM contributions other than multi-jet to the CRs, and the transfer factors, which relate the number of SM processes in their control regions to these predicted in the signal regions. The free parameters in the fit are the normalisations of the SM processes. The signal is assumed to be absent in the fit, and the SR is not included in the fit.
- A *model-independent* fit combines the data event yield in a given SR with the SM background estimate and its uncertainties obtained by the background-only fit to test whether any non-SM signal contributes to the SR. The significance of a possible excess of observed events over the SM prediction is quantified by the one-sided probability, $p(\text{signal} = 0)$ denoted by p_0, of the background alone to fluctuate to the observed number of events or higher using the asymptotic formula described in Ref. [86]. The presence of a non-SM signal would manifest itself in a small p_0 value. Values of $p_0 > 0.5$ correspond to a deficit of events and are truncated to $p_0 = 0.5$.
- In the *model-dependent* fit, the SUSY signal is taken into account in all regions and it is scaled by a floating signal normalisation factor. The background normalisation factors are also determined simultaneously in the fit. A SUSY model with a specific set of sparticle masses is rejected if the upper limit at 95 % confidence level (CL) of the signal normalisation factor obtained in this fit is smaller than the predicted cross-section of the model [87].

9.2 Intermediate stau analysis

9.2.1 SR yields

The observed number of events in each SR and the expected contributions from SM processes are given in Table 9. The contributions of multi-jet, W+jets and top events are scaled with the normalisation factors obtained from the background-only fit. The multi-jet normalisation with respect to the prediction from the ABCD method in all SRs is compatible with unity and has an uncertainty of around 29–40 % (4 %), due to the small number of observed events in the multi-jet CR-A in C1C1 and C1N2OS (C1N2SS) scenarios. The W+jets normalisation factor is measured to be 0.98 ± 0.12 (1.04 ± 0.09) in C1C1 and C1N2OS (C1N2SS) scenarios and the top normalisation factor is found to be 0.71 ± 0.11 in the C1N2SS scenario. The normalisation factors are summarised in Table 10. In all SRs, observations and background predictions are found to be compatible within uncertainties. The one-sided p_0-values, and the observed and expected

95 % CL upper limits on the visible non-SM cross-section (σ_{vis}^{95}) are shown. The accuracy of the limits obtained from the asymptotic formula was tested for all SRs by randomly generating a large number of pseudo-datasets and repeating the fit.

Table 9: Observed and expected numbers of events in the signal regions. The contributions of multi-jet and W+jets events are scaled with the normalisation factors obtained from the background-only fit. Expected event yields for the SUSY reference points defined in Section 6.1 are also shown. The uncertainties correspond to the sum in quadrature of statistical and systematic uncertainties. The correlation of systematic uncertainties among control regions and among background processes is taken into account. The one-sided p_0-values, and the observed and expected 95 % CL upper limits on the visible non-SM cross-section (σ_{vis}^{95}) are given.

SM process	SR-C1C1-LM	SR-C1C1-HM	SR-C1N2OS-LM	SR-C1N2OS-HM
Multi-boson	1.6 ± 0.6	2.2 ± 1.6	3.2 ± 1.2	2.4 ± 1.6
W+jets	0.4 ± 0.4	$0.29^{+0.35}_{-0.29}$	$0.6^{+2.2}_{-0.6}$	$0.29^{+0.35}_{-0.29}$
Top quark	1.0 ± 0.5	0.36 ± 0.13	$1.1^{+1.2}_{-1.1}$	0.36 ± 0.14
Z+jets	$1.4^{+1.5}_{-1.4}$	0.78 ± 0.34	2.5 ± 1.7	0.9 ± 0.4
Higgs	0.27 ± 0.06	$0.01^{+0.13}_{-0.01}$	0.40 ± 0.22	0.73 ± 0.23
Multi-jet	1.5 ± 0.5	0.37 ± 0.21	4.50 ± 0.97	0.31 ± 0.17
SM total	6.2 ± 2.0	4.0 ± 1.8	12.2 ± 4.8	5.0 ± 2.0
Observed	1	4	14	4
$m(\tilde{\chi}_1^{\pm}, \tilde{\chi}_1^0) = (700, 400)$ GeV	3.0 ± 0.6	7.8 ± 1.6	4.69 ± 0.99	14.1 ± 2.8
$m(\tilde{\chi}_1^{\pm}/\tilde{\chi}_2^0, \tilde{\chi}_1^0) = (1100, 0)$ GeV	0.20 ± 0.05	3.1 ± 0.6	0.39 ± 0.11	4.6 ± 1.0
p_0	0.5	0.5	0.4	0.5
Expected σ_{vis}^{95} [fb]	0.04	0.05	0.10	0.05
Observed σ_{vis}^{95} [fb]	0.02	0.05	0.10	0.05

SM process	SR-C1N2SS-LM	SR-C1N2SS-HM
Multi-boson	0.47 ± 0.20	0.8 ± 0.4
W+jets	0.33 ± 0.25	0.10 ± 0.05
Top quark	$0.01^{+0.02}_{-0.01}$	0.59 ± 0.20
Z+jets	0.20 ± 0.15	$0.6^{+0.8}_{-0.6}$
Higgs	$0.00^{+0.01}_{-0.00}$	0.02 ± 0.01
Multi-jet	0.9 ± 0.5	0.00 ± 0.00
SM total	2.0 ± 0.7	2.1 ± 1.1
Observed	2	3
$m(\tilde{\chi}_1^{\pm}/\tilde{\chi}_2^0, \tilde{\chi}_1^0) = (157, 92)$ GeV	4.6 ± 1.3	0.00 ± 0.00
p_0	0.4	0.3
Expected σ_{vis}^{95} [fb]	0.03	0.04
Observed σ_{vis}^{95} [fb]	0.03	0.04

9.2.2 Exclusion limits

In the absence of a significant excess over the expected SM background, the observed and expected numbers of events in the signal regions are used to place exclusion limits at 95 % CL using the model-dependent fit. SR-C1C1-LM and SR-C1C1-HM are statistically combined to derive limits on $\tilde{\chi}_1^+\tilde{\chi}_1^-$ production, and SR-C1N2OS-LM, SR-C1N2OS-HM, SR-C1N2SS-LM and SR-C1N2SS-HM are combined to derive limits for the production of $\tilde{\chi}_1^+\tilde{\chi}_1^-$ and $\tilde{\chi}_1^{\pm}\tilde{\chi}_2^0$. The exclusion limits for simplified models are shown in Figure 12. Only $\tilde{\chi}_1^+\tilde{\chi}_1^-$ production is assumed for Figure 12 (a), whereas both production processes are considered simultaneously for the Figure 12 (b) and (c). The C1N2SS channel contributes significantly to

Table 10: Normalisation factors from the background-only fit in each scenario. The normalisation factors include corrections to the mis-identified τ-lepton efficiency in addition to the cross-section and acceptance effects.

Normalisation factor	C1C1	C1N2OS	C1N2SS
$\mu_{W+\text{jets}}$	0.98 ± 0.12	0.98 ± 0.12	1.04 ± 0.09
$\mu_{\text{Multi-jet}}$	1.0 ± 0.4	1.00 ± 0.29	1.00 ± 0.04
μ_{Top}	-	-	0.71 ± 0.11

the combination in the lower mass regions where this channel does not contain significant SM backgrounds. In cases where the decay is via an intermediate stau, the stau mass is assumed to be half the sum of the $\tilde{\chi}_2^0$ / $\tilde{\chi}_1^\pm$ and $\tilde{\chi}_1^0$.

Chargino masses up to 970 GeV are excluded for decays to a massless neutralino in the direct production of chargino pairs. For production of chargino pairs of mass-degenerate charginos and next-to-lightest neutralinos, chargino masses up to 1160 GeV are excluded for a massless neutralino. Both limits apply to scenarios where the neutralinos and charginos decay solely via intermediate staus and τ sneutrinos. These limits significantly extend previous results [14, 15] in the high $\tilde{\chi}_1^\pm/\tilde{\chi}_2^0$ mass region. The improvement at compressed and low $\tilde{\chi}_1^\pm/\tilde{\chi}_2^0$ masses is mainly driven by the C1N2SS analysis contribution.

9.3 Intermediate Wh analysis

9.3.1 SR yields

The observed number of events in the two SRs and the expected contributions from SM processes are given in Table 11. The contribution of top events is scaled with the normalisation factor obtained from the background-only fit. The top normalisation factor is fitted to be 1.00 ± 0.14. In all SRs, the observed number of events from data and the background predictions are found to be compatible within uncertainties. The one-sided p_0-values, the observed and expected 95 % CL upper limits on the visible non-SM cross-section (σ_{vis}^{95}) are shown.

9.3.2 Exclusion limits

Since no significant excess over the expected SM background is observed, the observed and expected number of events in the SRs are used to place exclusion limits at 95 % CL using the model-dependent fit. The best expected limits for SR-Wh-LM and SR-Wh-HM are used to derive limits on $\tilde{\chi}_1^\pm\tilde{\chi}_2^0$ production decaying via an intermediate Wh, and are shown in Figure 13. Gaugino masses up to 330 GeV are excluded for a massless lightest neutralino.

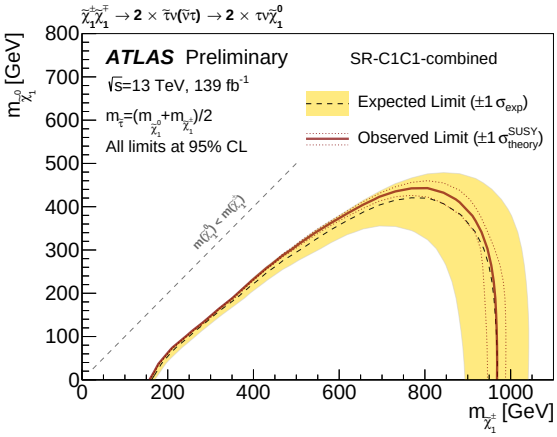

(a)

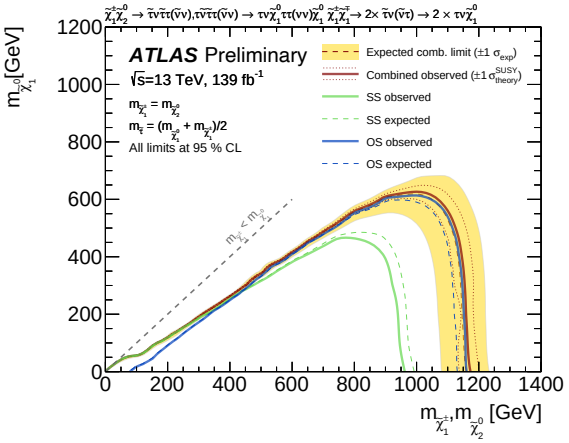

(b)

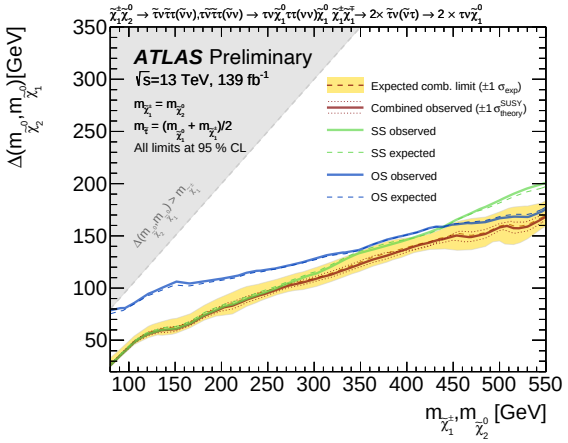

(c)

Figure 12: The 95 % CL exclusion contours for simplified models with $\tilde{\chi}_1^+\tilde{\chi}_1^-$ production (a) and production of $\tilde{\chi}_1^+\tilde{\chi}_1^-$ and $\tilde{\chi}_1^\pm\tilde{\chi}_2^0$ (b) and (c). The solid (dashed) lines show the observed (expected) exclusion contours. The band around the expected limit shows the $\pm 1\sigma$ variations, including all uncertainties except theoretical uncertainties in the signal cross-section. The dotted lines around the observed limit indicate the sensitivity to $\pm 1\sigma$ variations of the theoretical uncertainties in the signal cross-section. The green curves are from the contribution of C1N2SS scenario, while the blue curves are from the contribution of C1C1 and C1N2OS scenarios, and the red curves are the combination of the channels.

Table 11: Observed and expected numbers of events in the signal regions. The contribution from at least two misidentified τ-lepton events is estimated with the fake factor method. The contribution of top events is scaled with the normalisation factors obtained from the background-only fit. Expected event yields for the SUSY reference points defined in Section 7.1 are also shown. The uncertainties correspond to the sum in quadrature of statistical and systematic uncertainties. The correlation of systematic uncertainties among control regions and among background processes is fully taken into account. The one-sided p_0-values, and the observed and expected 95 % CL upper limits on the visible non-SM cross-section (σ^{95}_{vis}) are given.

SM process	SR-Wh-LM	SR-Wh-HM
Multi-boson	1.85 ± 0.5	1.1 ± 0.4
Misidentified processes	1.4 ± 0.6	0.06 ± 0.03
Top quark	1.9 ± 0.6	$0.04^{+0.06}_{-0.04}$
Z+jets	0.05 ± 0.02	0.03 ± 0.01
Higgs	$0.13^{+0.99}_{-0.13}$	0.06 ± 0.02
SM total	5.3 ± 1.4	1.3 ± 0.4
Observed	4	2
$m(\tilde{\chi}^{\pm}_1/\tilde{\chi}^0_2, \tilde{\chi}^0_1) = (225, 75)$ GeV	5.8 ± 1.5	3.3 ± 0.9
p_0	0.5	0.3
Expected σ^{95}_{vis} [fb]	0.05	0.03
Observed σ^{95}_{vis} [fb]	0.04	0.03

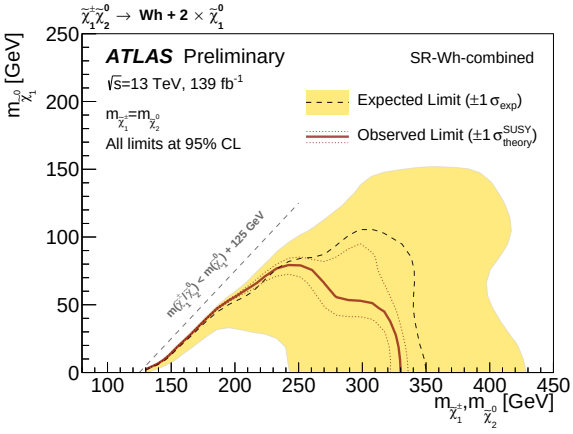

Figure 13: The 95 % CL exclusion contours for simplified models of $\tilde{\chi}^{\pm}_1\tilde{\chi}^0_2$ production decaying via an intermediate Wh. The solid (dashed) lines show the observed (expected) exclusion contours. The band around the expected limit shows the $\pm 1\sigma$ variations, including all uncertainties except theoretical uncertainties in the signal cross-section. The dotted lines around the observed limit indicate the sensitivity to $\pm 1\sigma$ variations of the theoretical uncertainties in the signal cross-section. The best expected limits for SR-Wh-LM and SR-Wh-HM are used.

10 Conclusion

Searches for direct gaugino pair production decaying via an intermediate stau or Wh with at least two hadronically decaying τ-leptons in the final state have been presented. The searches use 139 fb^{-1} of integrated luminosity of pp collisions at $\sqrt{s}$ = 13 TeV collected by the ATLAS detector from 2015 to 2018. Good agreement between data and SM expectation is observed in all signal regions. The results are used to set limits on the visible cross-section for events beyond the Standard Model.

Exclusion limits are placed for chargino masses up to 970 GeV for a massless lightest neutralino in the scenario of direct production of wino-like chargino pairs decaying into the lightest neutralino via an intermediate on-shell tau slepton. In the case of associated production of pairs of charginos and pairs of degenerate charginos and next-to-lightest neutralinos, masses up to 1160 GeV are excluded for a massless lightest neutralino. Using the full Run-2 dataset, the exclusion limits for high $\tilde{\chi}_1^{\pm}/\tilde{\chi}_2^0$ masses were improved by 340–400 GeV compared to the previous result. This improvement is mainly due to an increased amount of integrated luminosity and improvements in the recurrent neural network τ-lepton identification. The sensitivity at compressed $\tilde{\chi}_1^{\pm}/\tilde{\chi}_2^0$ mass region is also improved by the addition of the C1N2SS channel. For pairs of degenerate charginos and next-to-lightest neutralinos via Wh decay production, gaugino masses up to 330 GeV are excluded for a massless lightest neutralino. Gaugino masses up to 330 GeV are excluded for production of a lightest chargino and a next-to-lightest neutralino, both decaying via Wh, assuming the $\tilde{\chi}_1^{\pm}$ and $\tilde{\chi}_2^0$ have equal masses and the lightest neutralino is massless.

References

[1] Y. Golfand and E. Likhtman,
Extension of the Algebra of Poincare Group Generators and Violation of P Invariance,
JETP Lett. **13** (1971) 323, [Pisma Zh. Eksp. Teor. Fiz. **13** (1971) 452].

[2] D. Volkov and V. Akulov, *Is the neutrino a goldstone particle?*, Phys. Lett. B **46** (1973) 109.

[3] J. Wess and B. Zumino, *Supergauge transformations in four dimensions*,
Nucl. Phys. B **70** (1974) 39.

[4] J. Wess and B. Zumino, *Supergauge invariant extension of quantum electrodynamics*,
Nucl. Phys. B **78** (1974) 1.

[5] S. Ferrara and B. Zumino, *Supergauge invariant Yang-Mills theories*, Nucl. Phys. B **79** (1974) 413.

[6] A. Salam and J. Strathdee, *Super-symmetry and non-Abelian gauges*, Phys. Lett. B **51** (1974) 353.

[7] S. P. Martin, *A Supersymmetry Primer*, Adv. Ser. Direct. High Energy Phys. **18** (1998) 1,
arXiv: hep-ph/9709356.

[8] G. R. Farrar and P. Fayet, *Phenomenology of the production, decay, and detection of new hadronic states associated with supersymmetry*, Phys. Lett. B **76** (1978) 575.

[9] H. Goldberg, *Constraint on the Photino Mass from Cosmology*, Phys. Rev. Lett. **50** (1983) 1419,
Erratum: Phys. Rev. Lett. **103** (2009) 099905.

[10] J. Ellis, J. Hagelin, D. V. Nanopoulos, K. A. Olive and M. Srednicki,
Supersymmetric relics from the big bang, Nucl. Phys. B **238** (1984) 453.

[11] D. Albornoz Vásquez, G. Bélanger and C. Bœhm,
Revisiting light neutralino scenarios in the MSSM, Phys. Rev. D **84** (2011) 095015,
arXiv: 1108.1338 [hep-ph].

[12] ATLAS Collaboration, *Search for the direct production of charginos, neutralinos and staus in final states with at least two hadronically decaying taus and missing transverse momentum in pp collisions at $\sqrt{s} = 8$ TeV with the ATLAS detector*, JHEP **10** (2014) 096,
arXiv: 1407.0350 [hep-ex].

[13] ATLAS Collaboration, *Search for the electroweak production of supersymmetric particles in $\sqrt{s} = 8$ TeV pp collisions with the ATLAS detector*, Phys. Rev. D **93** (2016) 052002,
arXiv: 1509.07152 [hep-ex].

[14] ATLAS Collaboration, *Search for the direct production of charginos and neutralinos in final states with tau leptons in $\sqrt{s} = 13$ TeV pp collisions with the ATLAS detector*,
Eur. Phys. J. C **78** (2018) 154, arXiv: 1708.07875 [hep-ex].

[15] CMS Collaboration, *Search for electroweak production of charginos and neutralinos in proton–proton collisions at $\sqrt{s} = 13$ TeV*, JHEP **04** (2022) 147, arXiv: 2106.14246 [hep-ex].

[16] ATLAS Collaboration, *The ATLAS Experiment at the CERN Large Hadron Collider*,
JINST **3** (2008) S08003.

[17] ATLAS Collaboration, *The ATLAS Collaboration Software and Firmware*,
ATL-SOFT-PUB-2021-001, 2021, URL: https://cds.cern.ch/record/2767187.

[18] ATLAS Collaboration,
Luminosity determination in pp collisions at $\sqrt{s} = 13$ TeV using the ATLAS detector at the LHC,
ATLAS-CONF-2019-021, 2019, URL: https://cds.cern.ch/record/2677054.

[19] G. Avoni et al., *The new LUCID-2 detector for luminosity measurement and monitoring in ATLAS*,
JINST **13** (2018) 07017.

[20] ATLAS Collaboration, *ATLAS data quality operations and performance for 2015–2018 data-taking*,
JINST **15** (2020) P04003, arXiv: 1911.04632 [physics.ins-det].

[21] T. Sjöstrand, S. Mrenna and P. Z. Skands, *A brief introduction to PYTHIA 8.1*,
Comput. Phys. Commun. **178** (2008) 852, arXiv: 0710.3820 [hep-ph].

[22] ATLAS Collaboration, *The Pythia 8 A3 tune description of ATLAS minimum bias and inelastic measurements incorporating the Donnachie–Landshoff diffractive model*,
ATL-PHYS-PUB-2016-017, 2016, URL: https://cds.cern.ch/record/2206965.

[23] R. D. Ball et al., *Parton distributions with LHC data*, Nucl. Phys. B **867** (2013) 244,
arXiv: 1207.1303 [hep-ph].

[24] ATLAS Collaboration, *The ATLAS Simulation Infrastructure*, Eur. Phys. J. C **70** (2010) 823,
arXiv: 1005.4568 [physics.ins-det].

[25] GEANT4 Collaboration, S. Agostinelli et al., *GEANT4 – a simulation toolkit*,
Nucl. Instrum. Meth. A **506** (2003) 250.

[26] ATLAS Collaboration, *Performance of the Fast ATLAS Tracking Simulation (FATRAS) and the ATLAS Fast Calorimeter Simulation (FastCaloSim) with single particles*,
ATL-SOFT-PUB-2014-001, 2014, URL: https://cds.cern.ch/record/1669341.

[27] S. Frixione, P. Nason and G. Ridolfi,
A positive-weight next-to-leading-order Monte Carlo for heavy flavour hadroproduction,
JHEP **09** (2007) 126, arXiv: 0707.3088 [hep-ph].

[28] P. Nason, *A new method for combining NLO QCD with shower Monte Carlo algorithms*,
JHEP **11** (2004) 040, arXiv: hep-ph/0409146.

[29] S. Frixione, P. Nason and C. Oleari,
Matching NLO QCD computations with Parton Shower simulations: the POWHEG method,
JHEP **11** (2007) 070, arXiv: 0709.2092 [hep-ph].

[30] S. Alioli, P. Nason, C. Oleari and E. Re, *A general framework for implementing NLO calculations in shower Monte Carlo programs: the POWHEG BOX*, JHEP **06** (2010) 043,
arXiv: 1002.2581 [hep-ph].

[31] ATLAS Collaboration, *ATLAS Pythia 8 tunes to 7 TeV data*, ATL-PHYS-PUB-2014-021, 2014,
URL: https://cds.cern.ch/record/1966419.

[32] M. Beneke, P. Falgari, S. Klein and C. Schwinn,
Hadronic top-quark pair production with NNLL threshold resummation,
Nucl. Phys. B **855** (2012) 695, arXiv: 1109.1536 [hep-ph].

[33] M. Cacciari, M. Czakon, M. Mangano, A. Mitov and P. Nason, *Top-pair production at hadron colliders with next-to-next-to-leading logarithmic soft-gluon resummation*,
Phys. Lett. B **710** (2012) 612, arXiv: 1111.5869 [hep-ph].

[34] P. Bärnreuther, M. Czakon and A. Mitov, *Percent-Level-Precision Physics at the Tevatron: Next-to-Next-to-Leading Order QCD Corrections to $q\bar{q} \to t\bar{t} + X$*,
Phys. Rev. Lett. **109** (2012) 132001, arXiv: 1204.5201 [hep-ph].

[35] M. Czakon and A. Mitov,
NNLO corrections to top-pair production at hadron colliders: the all-fermionic scattering channels,
JHEP **12** (2012) 054, arXiv: 1207.0236 [hep-ph].

[36] M. Czakon and A. Mitov,
NNLO corrections to top pair production at hadron colliders: the quark-gluon reaction,
JHEP **01** (2013) 080, arXiv: 1210.6832 [hep-ph].

[37] M. Czakon, P. Fiedler and A. Mitov,
Total Top-Quark Pair-Production Cross Section at Hadron Colliders Through $O(\alpha_S^4)$,
Phys. Rev. Lett. **110** (2013) 252004, arXiv: 1303.6254 [hep-ph].

[38] M. Czakon and A. Mitov,
Top++: A program for the calculation of the top-pair cross-section at hadron colliders,
Comput. Phys. Commun. **185** (2014) 2930, arXiv: 1112.5675 [hep-ph].

[39] M. Aliev et al., *HATHOR – HAdronic Top and Heavy quarks crOss section calculatoR*,
Comput. Phys. Commun. **182** (2011) 1034, arXiv: 1007.1327 [hep-ph].

[40] P. Kant et al., *HatHor for single top-quark production: Updated predictions and uncertainty estimates for single top-quark production in hadronic collisions*,
Comput. Phys. Commun. **191** (2015) 74, arXiv: 1406.4403 [hep-ph].

[41] J. Alwall et al., *The automated computation of tree-level and next-to-leading order differential cross sections, and their matching to parton shower simulations*, JHEP **07** (2014) 079,
arXiv: 1405.0301 [hep-ph].

[42] A. Lazopoulos, T. McElmurry, K. Melnikov and F. Petriello,
Next-to-leading order QCD corrections to $t\bar{t}Z$ production at the LHC, Phys. Lett. B **666** (2008) 62,
arXiv: 0804.2220 [hep-ph].

[43] J. M. Campbell and R. K. Ellis, *$t\bar{t}W^{+-}$ production and decay at NLO*, JHEP **07** (2012) 052,
arXiv: 1204.5678 [hep-ph].

[44] T. Gleisberg et al., *Event generation with SHERPA 1.1*, JHEP **02** (2009) 007,
arXiv: 0811.4622 [hep-ph].

[45] S. Höche, F. Krauss, M. Schonherr and F. Siegert,
QCD matrix elements + parton showers: The NLO case, JHEP **04** (2013) 027,
arXiv: 1207.5030 [hep-ph].

[46] T. Gleisberg and S. Höche, *Comix, a new matrix element generator*, JHEP **12** (2008) 039,
arXiv: 0808.3674 [hep-ph].

[47] F. Cascioli, P. Maierhofer and S. Pozzorini, *Scattering Amplitudes with Open Loops*,
Phys. Rev. Lett. **108** (2012) 111601, arXiv: 1111.5206 [hep-ph].

[48] A. Denner, S. Dittmaier and L. Hofer,
Collier: a fortran-based Complex One-Loop LIbrary in Extended Regularizations,
Comput. Phys. Commun. **212** (2017) 220, arXiv: 1604.06792 [hep-ph].

[49] S. Schumann and F. Krauss,
A Parton shower algorithm based on Catani-Seymour dipole factorisation, JHEP **03** (2008) 038,
arXiv: 0709.1027 [hep-ph].

[50] R. D. Ball et al., *Parton distributions for the LHC Run II*, JHEP **04** (2015) 040,
arXiv: 1410.8849 [hep-ph].

[51] S. Catani, L. Cieri, G. Ferrera, D. de Florian and M. Grazzini, *Vector Boson Production at Hadron Colliders: A Fully Exclusive QCD Calculation at Next-to-Next-to-Leading Order*,
Phys. Rev. Lett. **103** (2009) 082001, arXiv: 0903.2120 [hep-ph].

[52] S. Höche, F. Krauss, M. Schonherr and F. Siegert,
A critical appraisal of NLO+PS matching methods, JHEP **09** (2012) 049,
arXiv: 1111.1220 [hep-ph].

[53] S. Catani, F. Krauss, R. Kuhn and B. R. Webber, *QCD matrix elements + parton showers*,
JHEP **11** (2001) 063, arXiv: hep-ph/0109231.

[54] S. Höche, F. Krauss, S. Schumann and F. Siegert, *QCD matrix elements and truncated showers*,
JHEP **05** (2009) 053, arXiv: 0903.1219 [hep-ph].

[55] D. de Florian et al.,
Handbook of LHC Higgs Cross Sections: 4. Deciphering the Nature of the Higgs Sector, 2016,
arXiv: 1610.07922 [hep-ph].

[56] D. J. Lange, *The EvtGen particle decay simulation package*,
Nucl. Instrum. Meth. A **462** (2001) 152.

[57] L. Lönnblad and S. Prestel, *Matching tree-level matrix elements with interleaved showers*,
JHEP **03** (2012) 019, arXiv: 1109.4829 [hep-ph].

[58] B. Fuks, M. Klasen, D. R. Lamprea and M. Rothering,
Gaugino production in proton-proton collisions at a center-of-mass energy of 8 TeV,
JHEP **10** (2012) 081, arXiv: 1207.2159 [hep-ph].

[59] B. Fuks, M. Klasen, D. R. Lamprea and M. Rothering,
Precision predictions for electroweak superpartner production at hadron colliders with RESUMMINO,
Eur. Phys. J. C **73** (2013) 2480, arXiv: 1304.0790 [hep-ph].

[60] C. Borschensky et al.,
Squark and gluino production cross sections in pp collisions at $\sqrt{s} = 13, 14, 33$ *and* 100 *TeV*,
Eur. Phys. J. C **74** (2014) 3174, arXiv: 1407.5066 [hep-ph].

[61] ATLAS Collaboration, *Vertex Reconstruction Performance of the ATLAS Detector at* $\sqrt{s} = 13$ *TeV*,
ATL-PHYS-PUB-2015-026, 2015, URL: https://cds.cern.ch/record/2037717.

[62] ATLAS Collaboration,
Jet reconstruction and performance using particle flow with the ATLAS Detector,
Eur. Phys. J. C **77** (2017) 466, arXiv: 1703.10485 [hep-ex].

[63] M. Cacciari, G. P. Salam and G. Soyez, *The anti-k_T jet clustering algorithm*, JHEP **04** (2008) 063,
arXiv: 0802.1189 [hep-ph].

[64] M. Cacciari, G. P. Salam and G. Soyez, *FastJet user manual*, Eur. Phys. J. C **72** (2012) 1896,
arXiv: 1111.6097 [hep-ph].

[65] ATLAS Collaboration,
Jet energy measurement with the ATLAS detector in proton–proton collisions at $\sqrt{s} = 7$ *TeV*,
Eur. Phys. J. C **73** (2013) 2304, arXiv: 1112.6426 [hep-ex].

[66] ATLAS Collaboration, *Jet Calibration and Systematic Uncertainties for Jets Reconstructed in the ATLAS Detector at* $\sqrt{s} = 13$ *TeV*, ATL-PHYS-PUB-2015-015, 2015,
URL: https://cds.cern.ch/record/2037613.

[67] M. Cacciari and G. P. Salam, *Pileup subtraction using jet areas*, Phys. Lett. B **659** (2008) 119,
arXiv: 0707.1378.

[68] ATLAS Collaboration, *Tagging and suppression of pileup jets with the ATLAS detector*,
ATLAS-CONF-2014-018, 2014, URL: https://cds.cern.ch/record/1700870.

[69] ATLAS Collaboration,
Optimisation and performance studies of the ATLAS b-tagging algorithms for the 2017-18 LHC run,
ATL-PHYS-PUB-2017-013, 2017, URL: https://cds.cern.ch/record/2273281.

[70] ATLAS Collaboration, *Electron and photon performance measurements with the ATLAS detector using the 2015–2017 LHC proton–proton collision data*, JINST **14** (2019) P12006,
arXiv: 1908.00005 [hep-ex].

[71] ATLAS Collaboration, *Muon reconstruction and identification efficiency in ATLAS using the full Run 2 pp collision data set at* $\sqrt{s} = 13$ *TeV*, Eur. Phys. J. C **81** (2021) 578,
arXiv: 2012.00578 [hep-ex].

[72] ATLAS Collaboration, *Measurement of the tau lepton reconstruction and identification performance in the ATLAS experiment using pp collisions at* $\sqrt{s} = 13$ *TeV*,
ATLAS-CONF-2017-029, 2017, URL: https://cds.cern.ch/record/2261772.

[73] ATLAS Collaboration, *Reconstruction, Energy Calibration, and Identification of Hadronically Decaying Tau Leptons in the ATLAS Experiment for Run-2 of the LHC*, ATL-PHYS-PUB-2015-045,
2015, URL: https://cds.cern.ch/record/2064383.

[74] ATLAS Collaboration,
Identification of hadronic tau lepton decays using neural networks in the ATLAS experiment,
ATL-PHYS-PUB-2019-033, 2019, URL: https://cds.cern.ch/record/2688062.

[75] ATLAS Collaboration, *Identification and energy calibration of hadronically decaying tau leptons with the ATLAS experiment in pp collisions at* $\sqrt{s} = 8$ *TeV*, Eur. Phys. J. C **75** (2015) 303, arXiv: 1412.7086 [hep-ex].

[76] ATLAS Collaboration, *Expected performance of missing transverse momentum reconstruction for the ATLAS detector at* $\sqrt{s} = 13$ *TeV*, ATL-PHYS-PUB-2015-023, 2015, URL: https://cds.cern.ch/record/2037700.

[77] ATLAS Collaboration, *Performance of missing transverse momentum reconstruction with the ATLAS detector in the first proton–proton collisions at* $\sqrt{s} = 13$ *TeV*, ATL-PHYS-PUB-2015-027, 2015, URL: https://cds.cern.ch/record/2037904.

[78] C. G. Lester and D. J. Summers, *Measuring masses of semi-invisibly decaying particles pair produced at hadron colliders*, Phys. Lett. B **463** (1999) 99, arXiv: hep-ph/9906349.

[79] A. Barr, C. Lester and P. Stephens, *A variable for measuring masses at hadron colliders when missing energy is expected; m_{T2}: the truth behind the glamour*, J. Phys. G **29** (2003) 2343, arXiv: hep-ph/0304226.

[80] ATLAS Collaboration, *Performance of the ATLAS muon triggers in Run 2*, JINST **15** (2020) P09015, arXiv: 2004.13447 [hep-ex].

[81] D. Tovey, *On measuring the masses of pair-produced semi-invisibly decaying particles at hadron colliders*, JHEP **04** (2008) 034, arXiv: 0802.2879.

[82] ATLAS Collaboration, *E_T^{miss} performance in the ATLAS detector using 2015–2016 LHC pp collisions*, ATLAS-CONF-2018-023, 2018, URL: https://cds.cern.ch/record/2625233.

[83] ATLAS Collaboration, *Measurement of the Inelastic Proton-Proton Cross Section at* $\sqrt{s} = 13$ *TeV with the ATLAS Detector at the LHC*, Phys. Rev. Lett. **117** (2016) 182002, arXiv: 1606.02625 [hep-ex].

[84] J. Butterworth et al., *PDF4LHC recommendations for LHC Run II*, J. Phys. G **43** (2016) 023001, arXiv: 1510.03865 [hep-ex].

[85] M. Baak et al., *HistFitter software framework for statistical data analysis*, Eur. Phys. J. C **75** (2015) 153, arXiv: 1410.1280 [hep-ex].

[86] G. Cowan, K. Cranmer, E. Gross and O. Vitells, *Asymptotic formulae for likelihood-based tests of new physics*, Eur. Phys. J. C **71** (2011) 1554, [Erratum: Eur. Phys. J. C **73** (2013) 2501], arXiv: 1007.1727 [physics.data-an], [Erratum: Eur. Phys. J. C **73** (2013) 2501].

[87] A. L. Read, *Presentation of search results: the CLs technique*, J. Phys. G **28** (2002) 2693.